PB86-236973

Ozone Formation in Pollutant Plumes A Reactive Plume Model with Arbitrary Crosswind Resolution

Washington Univ., St. Louis, MO

Prepared for

Environmental Protection Agency
Research Triangle Park, NC

Aug 86

U.S. Department of Commerce
National Technical Information Service
NTIS

PB86-236973

EPA/600/3-86/051
August 1986

OZONE FORMATION IN POLLUTANT PLUMES:

A REACTIVE PLUME MODEL WITH ARBITRARY CROSSWIND RESOLUTION

by

NOOR V. GILLANI

Mechanical Engineering Department
Washington University
St. Louis, MO 63130

EPA Co-operative Agreements No. CR-810372 and CR-809713

Project Officers

John F. Clarke, Francis Pooler Jr. and William E. Wilson
Atmospheric Sciences Research Laboratory
Research Triangle Park, North Carolina 27711

ATMOSPHERIC SCIENCES RESEARCH LABORATORY
OFFICE OF RESEARCH AND DEVELOPMENT
U.S. ENVIRONMENTAL PROTECTION AGENCY
RESEARCH TRIANGLE PARK, NC 27711

REPRODUCED BY
NATIONAL TECHNICAL
INFORMATION SERVICE
U.S. DEPARTMENT OF COMMERCE
SPRINGFIELD, VA. 22161

TECHNICAL REPORT DATA
(Please read Instructions on the reverse before completing)

1. REPORT NO.	2.	3. RECIPIENT'S ACCESSION NO.
EPA/600/3-86/051		PB86 236973/AS

4. TITLE AND SUBTITLE	5. REPORT DATE
OZONE FORMATION IN POLLUTANT PLUMES: A REACTIVE PLUME MODEL WITH ARBITRARY CROSSWIND RESOLUTION	August 1986
	6. PERFORMING ORGANIZATION CODE
7. AUTHOR(S)	8. PERFORMING ORGANIZATION REPORT NO.
Noor V. Gillani	
9. PERFORMING ORGANIZATION NAME AND ADDRESS	10. PROGRAM ELEMENT NO.
Mechanical Engineering Department Washington University St. Louis, MO 63130	CDWA1A/02 - 2063 (FY-86)
	11. CONTRACT/GRANT NO.
	Co-Operative Agreement No. CR-809713
12. SPONSORING AGENCY NAME AND ADDRESS	13. TYPE OF REPORT AND PERIOD COVERED
Atmospheric Sciences Research Laboratory--RTP, NC Office of Research and Development U.S. Environmental Protection Agency Research Triangle Park, NC 27711	Final
	14. SPONSORING AGENCY CODE
	EPA/600/09

15. SUPPLEMENTARY NOTES

16. ABSTRACT

A new two-layer reactive plume model is developed, in which arbitrary crosswind resolution of the emission field of each precursor is preserved, and dynamic plume-plume and plume-background interactions are explictly accomodated. The model has a hybrid formulation, having Lagrangian downwind transport and Eulerian crosswind spread. It is applied in a diagnostic mode to simulate the observed behavior of plumes of the metropolitan St. Louis area and the Labadie power plant. The RAPS emissions inventory gave detailed spatial resolution of the emission field, numerous stationary and mobile upper air wind soundings provided the basis for transport simulation, and aircraft data provided detailed crosswind profiles of pollutant concentrations across the plumes at downwind sections.

Background ozone and sulfate production were found to be NOx-limited, and poorly correlated with background NMHC/NOx. Power plant plume ozone and sulfate production were both positively correlated with background NMHC/NOx. Substantial excess ozone can form in a power plant plume without any interaction with a neighboring urban plume. Model simulations of ozone were generally good, even in crosswind detail, given an appropriate background characterization. Simulated values of the rate of SO_2 oxidation were quantitatively not as satisfying.

17. KEY WORDS AND DOCUMENT ANALYSIS

a. DESCRIPTORS	b. IDENTIFIERS/OPEN ENDED TERMS	c. COSATI Field/Group

18. DISTRIBUTION STATEMENT	19. SECURITY CLASS (This Report)	21. NO. OF PAGES
RELEASE TO PUBLIC	UNCLASSIFIED	138
	20. SECURITY CLASS (This page)	22. PRICE
	UNCLASSIFIED	

EPA Form 2220-1 (Rev. 4-77) PREVIOUS EDITION IS OBSOLETE

DISCLAIMER

The information in this document has been funded by the United States Environmental Protection Agency under Cooperative Agreements CR810372 and CR809713 to Washington University. It has been subjected to the Agency's peer and administrative review, and it has been approved for publication as an EPA document. Mention of trade names or commercial products does not constitute endorsement or recommendation for use.

ABSTRACT

In the summer, the atmospheric boundary layer over the eastern United States is substantially loaded with ozone and secondary sulfates and nitrates. The predominant source of the ozone is *in-situ* photosynthesis of anthropogenic emissions of the precursors NOx and NMHC (non-methane hydrocarbons) in plumes originating from urban-industrial complexes and power plants. The formation of ozone in such plumes typically leads to peak levels at short distances downwind of the major sources. Subsequently, the plumes gradually dilute into the regional airmass, thus contributing to the regional ozone burden.

In the past, official concern and control strategies for the abatement of the ozone problem have largely been focussed on the urban scale. Such strategies were directed mainly at controlling urban emissions of NMHC based on rather simple urban scale trajectory models (EKMA). Recently, the focus has shifted somewhat towards field measurements of regional ozone, and development of a sophisticated Eulerian regional oxidant model. Intermediate between the urban and the regional scales is the plume mesoscale. Peak ozone typically forms in this scale, and the effects of the spatial inhomogeneity of the precursor emission field (plume-plume interactions) and of the boundary conditions (plume-background interactions) are also significant in this scale. Their proper characterization in the regional models may be achieved through appropriate sub-grid scale parameterization. This report is focussed on the study of such mesoscale plume phenomena pertaining to ozone formation.

Field data are presented to demonstrate that, depending on meteorological conditions, fingerprints of the initial spatial inhomogeneity of a metropolitan source distribution can persist for many hours of summer daytime transport over 200 km and farther. Also, in a metropolitan plume composed of diverse individual plumes, the origin of the organic species involved in the photochemistry can range from almost all primary emissions to almost all background entrainment in different individual plumes. Evidently, the spatial inhomogeneities, lateral spread of the plume, and background entrainment, can be quite significant to ozone formation in plumes.

A new two-layer reactive plume model is developed, in which arbitrary crosswind resolution of the emission field of each precursor is preserved, and dynamic plume-plume and plume-background interactions are explictly accomodated. The model has a hybrid formulation, having Lagrangian downwind transport and Eulerian crosswind spread. It is applied in a diagnostic mode to simulate the observed behavior of the metropolitan plumes of St. Louis, MO on 9 July 1976 over a transport range of up to 200 km. For St. Louis, the RAPS emissions inventory gave detailed spatial resolution of the emission field, numerous stationary and mobile upper air wind soundings provided the basis for transport simulation, and aircraft data provided detailed crosswind profiles of pollutant concentrations across the plumes at downwind sections.

A detailed characterization of the background was obtained based on simultaneous simulation of the observed dynamics of ozone in the background and in the Labadie power plant plume. Background ozone and sulfate production were found to be NOx-limited, and poorly correlated

with background NMHC/NOx. On the other hand, power plant plume ozone and sulfate production were both positively correlated with background NMHC/NOx. Substantial excess ozone can form in a power plant plume without any interaction with a neighboring urban plume. About half of the ozone generation in the St. Louis plumes was in the power plant plumes. Power plant emissions of NOx, including those in rural locations, are a major contributor to the regional ozone burden in the eastern U.S. Their potency, however, is realized only because of the biased precursor loading of the regional background (NMHC/NOx around 30 ppbv/ppbv). This bias is a result of the strong disparity in the rates of consumption of NMHC and NOx in urban plumes. Model simulations of ozone were generally good, even in crosswind detail, given an appropriate background characterization. Simulated values of the rate of SO_2 oxidation were quantitatively not as satisfying.

The model described here is still in developmental stages. Its broad features have been established, but some details need significant further development. Further model validations based on field data also remain to be done.

CONTENTS

Abstract iii
Figures vii
Tables ix
Acknowledgements x

1. INTRODUCTION 1

2. FIELD OBSERVATIONS 6

2.1 Background 6
2.2 This Work 10

3. URBAN PLUME MODELLING 14

4. DESCRIPTION OF OUR MODEL 18

4.1 Overview 18
4.2 Mathematical Formulation 21
4.2.1 Basic Equation for Plume Pillar i, Species j
4.2.2 Basic Equations for Background and Aloft
4.2.3 Initial and Boundary Conditions
4.3 The Chemical Scheme 27
4.4 Dry Deposition 29
4.5 Numerical Analysis 30

5. TESTING OF MODULES 36

5.1 Crosswind Dispersion Module 36
5.2 Chemistry Module 39

6. MODEL APPLICATION 40

6.1 Plume Transport Simulation 40
6.2 Characterization of the Ambient Environment 44
6.3 Sensitivity of Power Plant Plume Ozone to Ambient Air Composition 54
6.4 Sensitivity of Ambient and Plume Sulfur Chemistry to Ambient Air Composition 57
6.5 Model Application to the Metropolitan Plume 62

7. SUMMARY AND CONCLUSIONS 75

7.1 Principal Features of the New Model 76
7.2 Goals of Model Application 77
7.3 Results of Model Application 78
7.3.1 Ambient Environment
7.3.2 Power Plant Plumes
7.3.3 Metropolitan Plumes
7.3.4 General

REFERENCES 82

FIGURES

Number		Page
1.	Spatial distribution of the average summertime anthropogenic emissions of NOx and THC (total hydrocarbons) during the morning rush period in metropolitan St. Louis, MO (c. 1975) according to the RAPS emisssions inventory.....	7
2.	The St. Louis metropolitan area, major point sources, the emissions profiles of the precursors (NOx, NMHC), and the crosswind profiles of SO_2 and ozone in the metropolitan plume based on two downwind aircraft traverses.....	11
3.	Illustration of the coordinate system and of some model features in the time-height and horizontal planes.....	20
4.	Test of numerical accuracy of the crosswind dispersion module for a scenario of known analytical solution for a complex 3-source release into a steady-state meteorological environment.....	37
5.	Monte Carlo transport of point releases from Labadie at 1200 and from Wood River at 1500 for 9 July 1976.....	41
6.	Some dynamic input variables of the model for 9 July 1976.....	42
7.	Spatial-temporal variation of ambient NMHC in the vicinity of Columbus, OH based on measurements of Project PEPE/NEROS.....	47
8.	Standard run model simulation of the precursors and of ozone in the ambient airmass of 9 July 1976 near St. Louis.....	50
9.	Influence of entrainment from aloft on ambient ozone in the mixing layer.....	52
10.	Sensitivity of background ozone in the mixing layer to regional emission flux of the precursors...	53
11.	Evolution of simulated crosswind profiles of the Labadie power plant plume for 9 July 1976, corresponding to the three different cases of regional emissions of NOx and NMHC.....	56
12.	Dynamics of plume-average ozone in the Labadie plume of 9 July 1976 corresponding to the three cases of regional emissions of NOx and NMHC.....	58

Number		Page
13.	Dynamics of OH, HO_2, and H_2O_2 in the ambient aloft and mixing layer air, and of plume-average OH and HO_2 in the Labadie plume, corresponding to the three cases of regional emissions of NOx and NMHC	60
14.	Rate of SO_2 oxidation in the background and in the Labadie plume, corresponding to the three cases of regional emissions of NOx and NMHC	61
15.	Initial concentration profiles of the precursors for two metro St. Louis model runs	63
16.	Evolution of simulated crosswind ozone profiles for emissions scenarios 1c and 2c of the St. Louis metro plume run for 9 July 1976	67
17.	Dynamics of simulated concentrations of NMHC and aldehydes in the background and near the cores of the Labadie and urban plumes for the emissions scenarios 1c and 2c	69
18.	Dynamics of simulated concentrations of NOx, HNO_3, and PAN in the background and near the cores of the Labadie and urban plumes for the emissions scenarios 1c and 2c	70
19.	Dynamics of simulated concentration of O_3 and the rate of oxidation of SO_2 in the background and in the cores of the Labadie and urban plumes for the emissions scenarios 1c and 2c	72
20.	Dynamics of simulated concentrations of OH, HO_2 and H_2O_2 in the background and near the cores of the Labadie and urban plumes for the emissions scenarios 1c and 2c	74

TABLES

Number		Page
1.	Ambient initial concentrations of trace species at 0600	49
2.	Summary of primary emissions scenarios for metropolitan plume runs	11

ACKNOWLEDGEMENTS

This research was supported jointly by EPA Co-operative Agreements CR-810372 and CR-809713. We gratefully acknowledge this support. We are grateful also to Dr. Warren H. White and David E. Patterson of Washington University for permission to adapt our Figure 2 from their previous research, for the use of the computer codes used to generate Figure 1, and to perform the Monte Carlo plume transport simulations.

1. INTRODUCTION

The debate concerning the relative contributions to tropospheric ozone by *in-situ* photochemical synthesis and by stratospheric input continues. It is increasingly evident, however, that at least in the Northern Hemisphere, *in-situ* production is the dominant source of ozone (Fishman and Crutzen, 1978). Also, much of the *in-situ* production of ozone in the Northern Hemisphere is localized in certain industrialized regions where the anthropogenic emissions of precursors are most concentrated. A recent analysis of available ozone data in the eastern United States indicates the existence of a substantial reservoir of ozone in the boundary layer in summertime (Vukovich et al, 1985). Measured vertical profiles of ozone in the lower troposphere in this region also show peak ozone concentrations to be within the boundary layer during the photochemically active period on summer afternoons, indicating a corresponding net upward flux of ozone from the boundary layer to the free troposphere (Vukovich et al, 1985; Fishman et al, 1985). These observations are consistent with mesoscale field observations of substantial amounts of ozone formation in pollutant plumes originating from urban-industrial complexes (White et al, 1976; 1983; Wolff et al, 1977; Spicer et al, 1979; 1981; 1982), and from large power plants (Miller et al, 1978; Gillani and Wilson, 1980). White et al (1983) estimated that the rate of photochemical synthesis of ozone in the urban plume of St. Louis on summer days promptly reaches a peak level roughly equivalent to the average summertime rate of stratospheric input over an area of about one-third of the eastern United States. Such concentrated mesoscale generation of ozone in pollutant plumes frequently leads to local levels well in excess of the 120 ppb U.S. National Ambient Air Quality Standard (NAAQS), and has local impact severe enough to cause observable damage to human health, forests and crops, and materials. In addition, it also influences the regional and global ozone budgets.

High levels of ozone generated rapidly in pollutant plumes during the daytime frequently remain trapped at night in layers aloft which are decoupled from ground removal, and are thus transported over a long

range. The next morning, such ozone may be entrained into the mixing layer, thereby contributing to a potentially cumulative multiday build-up. The build-up of ozone in pollutant plumes depends on chemical factors, meteorological factors, and removal mechanisms. Together, these factors determine the concentrations of precursors and oxidants involved in the photochemical cycle of smog formation. Chemical factors include concentrated primary emissions of the precursors, as well as entrainment of influencing anthropogenic and natural species from the background and from aloft. The cornerstone of EPA's regulatory program for the attainment of ozone NAAQS has been the reduction of urban anthropogenic emissions of reactive organic precursors based on urban scale photochemical air quality simulation models (PAQSM). A major current EPA effort focuses on the development of a regional PAQSM (Schere and Possiel, 1984). However, given the concentrated nature of precursor emissions and the promptness with which ozone forms during peak periods, proper subgrid scale parameterization of urban plume contribution to regional ozone may be of critical importance in regional models. Thus, the subject of first day ozone generation in metropolitan and power plant plumes remains important in terms of both local and regional impact.

Most of the data base pertaining to the sensitivity of ozone formation to precursors is derived from controlled smog chamber studies involving measurements of reactants and products in artificially irradiated precursor mixtures. Even if the level of irradiation, and temperature and humidity effects, are controlled to simulate realistic atmospheric conditions, other critical meteorological factors such as dilution of the precursors by day-specific entrainment of time-varying background and aloft are generally not duplicated in laboratory simulations. For a proper understanding of the combined role of chemical and meteorological factors, appropriate *in-situ* field data are invaluable. Since field measurements are generally not exhaustive, the use of appropriate numerical models can facilitate more thorough interpretations and sometimes also meaningful extrapolations. Early models of urban ozone prediction, popular as late as in the early 1970's, were statistical and empirical in nature, relating maximum daily

urban ozone to morning rush-hour precursor levels based on air monitoring data (Schuck et al, 1970). These models have now been supplanted by dynamic models based on the Empirical Kinetic Mechanism Approach, EKMA (EPA 1977b; 1978; Whitten and Hogo, 1978). EKMA conceptually involves dynamic computation of ozone generation within an urban area based on a mechanism of smog chemistry applied to a mixture of morning rush-hour primary emissions injected into air advected from upwind. As the reacting mixture is transported, it is allowed to intake subsequent emissions along the trajectory, and to dilute within a single Lagrangian box which grows vertically and entrains air from aloft. The chemical mechanisms used in such models are usually validated by specific dynamic smog chamber data sets. EKMA may be implemented in a day- and city-specific mode by input of appropriate initial conditions pertaining to upwind and aloft air, and of dynamic conditions pertaining to insolation, mixing layer growth, plume trajectory, and downwind emissions (EPA, 1980). Applications of EKMA models do not include the effect of ground removal. The methodology of implementation of EKMA consists of multiple simulations to construct a family of peak afternoon ozone isopleths as a function of initial composition of precursor nonmethane hydrocarbons (NMHC) and nitrogen oxides (NOx).

Even the city-specific implementation of EKMA involves many assumptions and approximations which strictly restrict the validity of the results to worst-case scenarios. More refined urban plume models include the SAI Urban Airshed Model (Reynolds and Reid, 1978; Reynolds et al, 1979), which is a sophisticated grid model that is often more demanding in input requirements than are available presently in the case of most cities. It is also computationally demanding. Validations of city-specific EKMA based on field observations are few, and those based on comparison with more resolved and refined models are sometimes based on input information which is inadequate for the refined models.

One significant simplification in EKMA is the coarseness of its crosswind resolution. The emissions are assumed to be uniformly distributed initially and subsequently into a single box. Large cities are commonly characterized by very non-uniform spatial distributions of

the ratio of nonmethane hydrocarbons to nitrogen oxides (NMHC/NOx) in the primary emissions. The reactivity of the organic vapors in terms of potential for ozone production is well-known to be very sensitive to this ratio (see, for example, Dodge, 1984). Also, the HC-NOx photochemistry which is reponsible for ozone production is highly non-linear. Hence, applications of EKMA must be limited to short range transport of emissions from subsections of an urban complex. In spite of such limitations, appropriate application of EKMA can give predictions of peak daily ozone in urban plumes in surprising agreement with corresponding results from the application of the Urban Airshed Model (UAM) even when the same chemical mechanism is used in both model calculations (see, for example, Gipson, 1984). When the daily ozone peak in the plume occurs substantially downwind of the metropolitan area, the effects of the spatial-temporal inhomogeneities of the urban precursor emissions and of plume-background interactions become significant, and a proper simulation requires finer crosswind resolution and incorporation of lateral dispersion.

The research presented in this paper represents the initial part of an attempt to utilize detailed mesoscale meteorological and chemical field data, in conjunction with finely resolved urban emissions data and a new crosswind-resolved reactive plume model, to investigate the sensitivity of ozone formation in power plant and urban plumes to non-homogeneous precursor emissions and to the chemical composition of the background. The field observations presented here are for the St. Louis metropolitan plumes on a particular summer day when background entrainment played a critical role in ozone formation in the Labadie power plant plume as it was transported alongside, and more or less isolated from, the more complex main urban plume incorporating interacting emissions from a variety of stationary and mobile sources. The new model is described. Conceptually and computationally, it represents a level of refinement which is intermediate between the city-specific EKMA and the UAM. The important questions of background characterization and ozone generation in a power plant plume are particularly emphasized here. The model is still in a developmental stage. Its potential as a research tool is examined through some

preliminary sensitivity analyses. Plans for its future development are outlined.

2. FIELD OBSERVATIONS

2.1 Background

Field measurements of ozone production in pollutant plumes have been reported downwind of many cities (St. Louis, Los Angeles, Chicago, Houston, Boston-Washington Northeast Corridor, Milwaukee, Springfield [IL], and others), oil refineries, various industrial plants, and power plants (see, for example, Clark and Clarke (1984); EPA, 1977a; Gillani and Wilson, 1980; Miller et al, 1978; Miller and Alkezweeny, 1980; Sexton and Westberg, 1983; Spicer et al, 1979; 1982; White et al, 1976; 1983; Wolff et al, 1977). Some general observations of these studies are summarized below:

- ozone generation in pollutant plumes is more or less in accordance with the traditional understanding of photochemical smog chemistry;
- net ozone formation occurs when the ratio NMHC(ppbC)/NOx(ppb) is typically in the range 5 to 20;
- the rate of ozone production is related to the composition of the hydrocarbons;
- superposition of emissions from different sources (source intensification) often leads to enhanced ozone generation;
- composition of the entrained background air can play an important role in power plant as well as urban plume ozone production.

In this study, some of the St. Louis data have been re-examined in a more quantitative and detailed manner than in the past. St. Louis is a major urban-industrial center, encompassing coal-fired power plants with aggregate capacity of about 5000 MWe, oil refineries with aggregate capacity of nearly 0.5 million barrels/day, a variety of heavy industry, a population of over 2 million, and a corresponding large transportation-related source of ozone precursors (NHMC and NOx). St. Louis pollutant emissions were inventoried with unusually detailed effort and spatial resolution as part of the Regional Air Pollution Study (Strothman and Schiermeier, 1979). Figure 1 shows the spatial

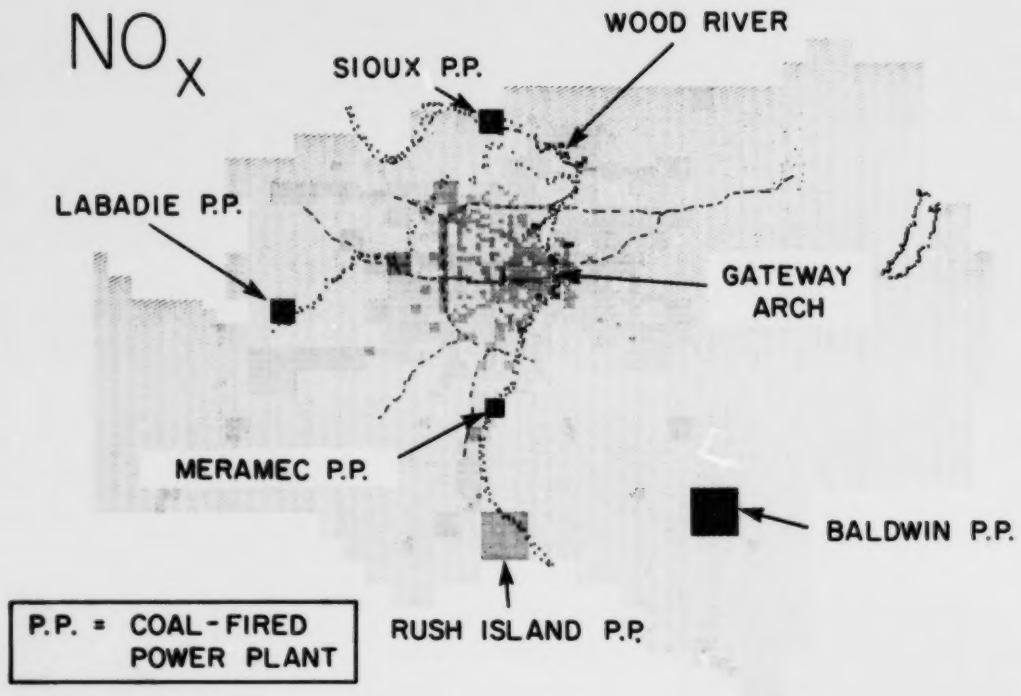

Figure 1. Spatial distribution of the average summertime anthropogenic emissions of NOx and THC (total hydrocarbons) during the morning rush period in metropolitan St. Louis, MO (c. 1975) according to the RAPS emisssions inventory. The outermost shaded area represents the spatial domain of the gridded region which was inventoried. The darker shadings depict the intensity of the emissions flux from each of the grid cells, and is on a grey scale with black denoting the highest flux. The square grid cells range in dimension from 1 km side in the central business district area near the Gateway Arch to 10 km side in the outer region of the gridded domain.

distributions of the anthropogenic morning rush-hour emissions of NOx and THC (total hydrocarbons) in St. Louis based on the RAPS emissions inventory. In this study, St. Louis emissions are estimated (c. 1975) to be about 30 T(NOx)/h (expressed as NO_2), 35 T(NMHC)/h, and 100 T(SO_2)/h during an average summer day (T = metric tons). Of particular interest in this study are the Labadie and Sioux coal-fired power plants (major sources of SO_2 and NOx), and the Wood River petroleum refinery complex (major source of SO_2, NOx, and NMHC). In addition, NOx and HC sources also show a broad aerial coverage.

The choice of St. Louis as the base of the RAPS measurements was motivated by its size and emissions, relative isolation from other major population and industrial centers, and by its surrounding flat terrain. Clearly identifiable St. Louis plumes have, on occasions, been sampled from aircraft out to distances in excess of 300 km as part of the MISTT measurement program (Gillani et al, 1978). Such occasions provide a particularly good opportunity to study the formation of ozone in plumes, because they include not only the afternoon period of ozone build-up to its peak level, but also the subsequent drop in the evening when the photochemical production and removal cease, while its chemical depletion and physical dilution continue.

During the MISTT field studies in St. Louis during the summers of 1975 and 1976 (see Gillani and Wilson, 1985 for a detailed description of the MISTT measurements program and the data base), *in-situ* aircraft measurements were made in power plant and urban plumes, and closely-coordinated supporting upper air wind soundings were made in a mobile mode along the plume trajectories. Continuous aircraft measurements normally included gaseous parameters (SO_2, NO, NOx, O_3), aerosol parameters (CNC, aerosol charge, B_{scat}), meteorological parameters (ambient and dewpoint temperature, turbulence), and navigational parameters. Unfortunately, however, on the particular day of focus in this study (9 July 1976), one of the two sampling aircraft was not operational, and the aircraft in operation did not measure NO, NOx and turbulence. In addition, intensive chemical and meteorological monitoring data were collected in the metropolitan area as part of RAPS.

Further supporting measurements of RAPS included frequent upper air soundings of temperature, humidity, and wind speed and direction at four fixed stations in and around St. Louis.

Investigation of ozone formation in the Labadie power plant plume has previously revealed a consistent evolutionary pattern of three distinct chemical stages (Gillani and Wilson, 1980): an early stage dominated by ozone depletion in the plume by reaction with primary NO; an intermediate stage showing clearly the critical role of background entrainment of organic species in the recovery and build-up of ozone in the plume, proceeding from plume edges toward the core; and the final stage characterized by a distinct plume of excess ozone with the peak in the core. The same pattern of ozone formation was also observed by the authors in measurements made in the Cumberland power plant plume in the Tennessee-Kentucky area in a later field study also in the summer (Gillani et al, 1981). The interpretation advanced by the authors was that the regional background in the eastern United States must contain a sufficiently large reservoir of reactive organic species and their photochemical breakdown products, such that the limitation to ozone production in this region is the availability of NOx. Injection of NOx from power plants into such a background ultimately leads to net ozone generation following an initial depletion of background ozone within the fresh plume. Net generation of ozone in power plant plumes in the eastern United States on summer afternoons was believed by the authors to be the rule rather than the exception as claimed in several prior studies over shorter transport ranges not covering all three stages of plume development.

Investigation of ozone generation in the metropolitan plume of St. Louis on three different summer days (White et al, 1983) revealed rapid ozone generation after the initial hour or so of transport, and attainment of peak ozone condition during the afternoon within a few

hours from the urban source. For St. Louis, the peak ozone burden was equivalent to "virtual emission rates"* of 100 to 150 T/h.

2.2 This Work

In this work, we re-examine the data of St. Louis for 9 July 1976 which have previously been studied by Gillani (1978) and Gillani et al (1978) with respect to sulfur chemistry in the Labadie plume, and by White et al (1983) with respect to ozone and aerosol formation in the metropolitan plume. Meteorologically, the day was very sunny, boundary layer relative humidity remained generally under 75%, and the maximum ground level temperature exceeded 30°C. Figure 2 (upper) shows the St. Louis source region and the measured crosswind profiles of SO_2 (primary) and ozone (secondary) for two downwind aircraft traverses. The first traverse (A-A) was made within the well-mixed boundary layer at about 1600. The Labadie plume in that traverse is estimated to be approximately 5 hours old, and the urban plume about 3 to 4 hours old. The Labadie and Sioux power plant plumes are in a diluted state, both showing peak ozone concentrations similar to that in the urban plume (about 140 ppb compared to background ozone around 70 ppb). The corresponding virtual emission rate of ozone for the entire metropolitan plume was estimated by White et al (1983) at about 100 T/h. Observe that at least half of this net ozone formation is in the power plant plumes. Figure 2 (lower) duplicates the measured ozone profile of the 1600 traverse, and also depicts the spatial distribution of the primary emission of THC and NOx. The profiles for these precursors represent downwind concentrations at the location of the 1600 traverse obtained by passive advection (assuming species to be inert and conservative) of their emissions based on the RAPS emissions inventory data and the measured prevailing wind data. It is clear that the initial HC/NOx based on primary emissions is relatively high in the urban plume and low in the power plant plumes, particularly in the Labadie plume. In spite of such strong spatial inhomogeneity in the precursor emissions fields,

---

(*) Virtual emission rate of ozone is defined as that hypothetical primary emission rate which would give the observed downwind concentration field if ozone were a conservative primary species.

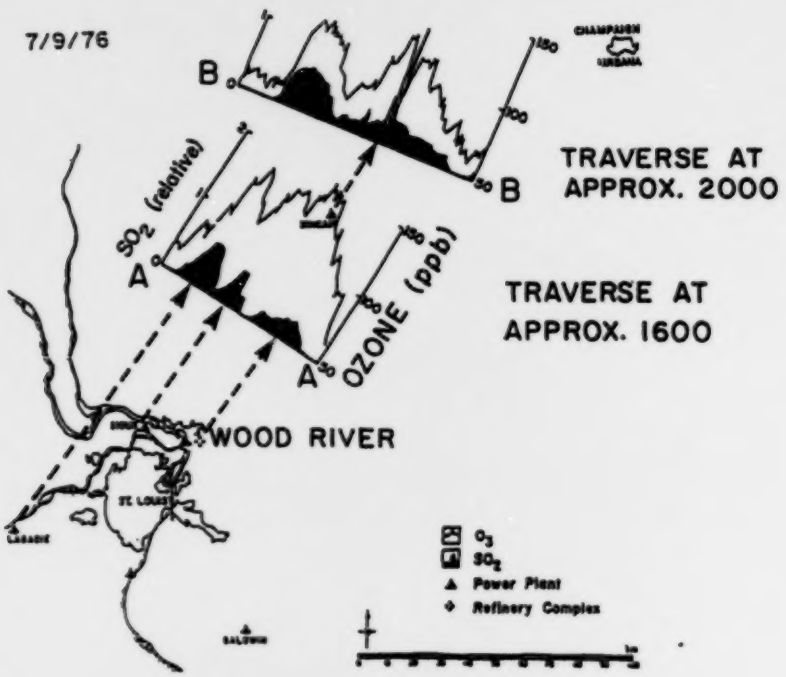

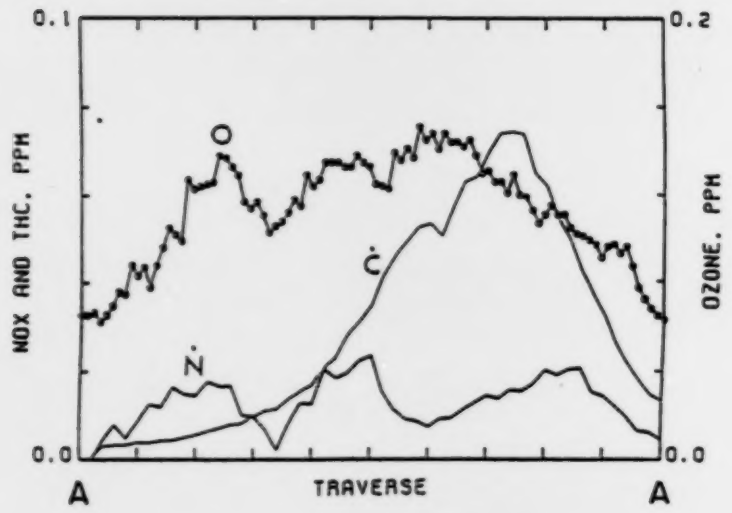

Figure 2. (Upper) The St. Louis metropolitan area, major point sources, and the crosswind profiles of SO_2 and ozone in the metropolitan plume based on two downwind aircraft traverses.
(Lower) The observed crosswind profile of ozone in the 1600 aircraft traverse, and the simulated profiles of primary NOx and THC also at this location. These precursor profiles are based on simulated conservative transport of their metropolitan emissions according to the RAPS emissions inventory data. The transport simulation is based on a Monte Carlo technique and used measured RAPS and MISTT upper air wind data. (This figure is adapted from a figure in White and Patterson, 1983).

ozone generation is of comparable magnitude across the entire metropolitan plume. The second downwind traverse (B-B) in Figure 2 (upper) shows crosswind profiles of SO_2 and ozone measured at approximately 2000 in the aged metropolitan plume in the nocturnal aloft layers. The two traverses shown are not Lagrangian. The Labadie plume in the 2000 traverse represents approximately the 1200 release and the Wood River release in the corresponding urban plume is estimated to be at about 1500. There is little evidence of material interaction between the Labadie plume and the remainder of the metropolitan plume in this case. Evidently, the necessary organic precursors involved in the observed rapid ozone production in the Labadie plume did not originate significantly from primary emissions in St. Louis, but rather were entrained from the regional background. Thus, in industrialized regions such as the eastern United States, the regional background is an important source of reactive organic matter which can boost the ozone forming potential of rural power plant emissions to levels comparable with those of urban-industrial emissions.

The crosswind-resolved aircraft data, particularly of the 2000 traverse, provide an excellent indication of the significance of both primary emissions and entrainment from the surroundings as important contributors to plume ozone generation. For proper quantitative interpretation of this observation, and to gain furthur insight into the relative importance of primary emissions and background entrainment, an ideal tool would be a crosswind-resolved reactive plume model which can explicitly retain the inhomogeneity of spatial distribution of emissions, and be capable of facilitating realistic plume spread and interaction with a dynamic environment. On 9 July 1976, the plume environment was indeed dynamic: within the boundary layer, background ozone concentration increased from about 25 ppb early in the morning to about 75 ppb in the afternoon, and then decreased to less than 65 ppb by the time of the 2000 traverse; above the mixing layer, the concentration increased from about 40 ppb at 0800 to nearly 60 ppb by noontime. Afternoon mixing layer height reached up to a maximum of about 1250 m.

To provide an appropriate framework for interpretation of such data, we have developed a new reactive plume model with the necessary

crosswind resolution. It is a hybrid model combining Lagrangian transport within an expanding crosswind grid. The model treats both elevated power plant releases and near-surface urban releases, and distinguishes between the mixing layer and the aloft layer. The model is applied to simulate the observations of the 2000 aircraft traverse across the St. Louis metropolitan plume in the nocturnal aloft layer at a downwind distance of 150-200 km from the source. A brief overview of urban plume modelling is given in the next section. The current state of our new model, and its test and preliminary applications are described in subsequent sections.

3. URBAN PLUME MODELLING

Photochemical air quality simulation models for urban plumes vary mainly in terms of the type of mathematical formulation, the specific choice of the chemical mechanism, and the method of numerical integration of the model equations.

The mathematical formulation is governed by the chosen frame of reference (Eulerian or Lagrangian), the spatial-temporal resolution (integral or differential), and the initial and boundary conditions. In Eulerian air pollution models, plume transport is within a gridded domain. Concentrations of all simulated species must be specified for all grid cells initially, and at the boundaries for all subsequent times. Inputs for meteorological variables are required dynamically for all grid cells. The differential mathematical formulation consists of the set of simultaneous differential mass continuity equations for all species applicable in each cell. Each differential equation includes individual terms representing each physical and chemical process instantaneously influencing species concentrations in each cell. The solution yields dynamic snap-shots of the spatial distributions of species concentrations over the entire gridded domain. Such models can be extremely demanding in terms of input requirements and computational resources. As a compromise in practice, either the grid resolution, or the chemical speciation, or both, may be coarse. The simplest example of such a model is the EPA Photochemical Box Model, PBM (Demerjian and Schere, 1979). It consists of a single well-mixed cell which is large enough to occupy the whole city surface area, and its vertical domain is equal to, and variable as, the mixing layer height. Entrainment from aloft is permitted. Such a limited spatial resolution restricts the application of this model only to stagnant conditions when the reactive urban plume remains resident and well-mixed within the model box. The original PBM model used a chemical scheme based on 24 variable species and 36 reactions simulating the NOx-HC photochemistry. The reactive hydrocarbons were lumped into four molecular reactivity classes (olefins, aromatics, paraffins and aldehydes). The products included O_3, HNO_3, and PAN. Sulfur chemistry was not included.

Representative of the more complex grid models is the SAI-UAM mentioned previously. One application of it to St. Louis (Gipson, 1984), for example, covered a 60 km by 80 km horizontal domain resolved into square grid cells of 4 km sides. Four vertical cells included the mixing layer (2 cells) and the layers aloft up to a maximum height of 2 km above ground. The gridded domain included a stretch of less than 20 km downwind of the refinery complex at Wood River for the predominant southwesterly flow of summer days. Hence, it may well not include the location of the global maximum ozone formation in the plume on most summer days. The application of the model at such spatial resolution over a domain extending 200 km downwind of the sources would be computationally very much more elaborate. The gridded domain in the example application also did not include the Labadie power plant which is a major point source of SO_2 and NO in the St. Louis region, and a major contributor to the overall metropolitan oxidant impact downwind. On occasions, the Labadie plume merges with the urban plume, and substantially modifies the HC/NOx values. In applications of the UAM such as the above, the proper inclusion of Labadie in the boundary conditions on such occasions must be of critical importance.
The UAM uses a chemical scheme based on the (CBM) carbon-bond mechanism (Killus and Whitten, 1982) in which submolecular structures (the carbon bonds) are used as the basic reacting units rather than the molecules themselves. In a recent application of the UAM to Los Angeles, Killus and Whitten (1984) tested model sensitivity to the chemical mechanism by implementing both the CBM-II and the Demerjian-Schere (DS-PBM) schemes in the UAM. Both schemes gave simulated ozone in the surface layer which was in good agreement with surface monitoring data. The DS-PBM mechanism generally predicted slightly higher ozone values than did the CBM-II.

Lagrangian or trajectory models attempt to simulate the dynamics and kinetics of a given source release within an identified air parcel as it is transported along a particular trajectory. The air parcel may expand in time and entrain material from its surroundings. The city-specific EKMA models are of this type. As mentioned previously, EKMA models lack spatial resolution and the ability to expand laterally. Refinements are

typically aimed at these shortcomings. Some trajectory models are applied to a well-mixed box which can expand laterally also and entrain the background (Bazzell and Peters, 1981; Miller and Alkezweeny, 1980). Crosswind-resolved reactive plume models, using two vertical layers (well-mixed boundary layer and an aloft layer), have been developed for application specifically to power plant plumes (Hov and Isaksen, 1981; Stewart and Liu, 1981). These models assume similar (Gaussian) profiles of all primary emissions. The profiles are also assumed to be symmetric about plume centerline. While these models are capable of simulating lateral plume expansion and the important role of background entrainment in power plant plume chemical evolution, they cannot simulate arbitrary, spatially inhomogeneous and non-similar profiles of the primary emissions. Thus, they are inappropriate for application to most metropolitan plumes.

Two trajectory models provide spatial resolution only in the vertical direction. These are the ERT-LPM (Lagrangian Photochemical Model, also called PLMSTAR in its current most developed form) and the SAI-ACTM (Airshed-Compatible Trajectory Model). The original LPM (Lurman et al, 1979) was fixed in size laterally, but possessed multiple vertical layers into which downwind surface emissions mixed at a finite rate. With the improved vertical resolution, however, unrealistic assumptions were made concerning the initial vertical conditions of the precursors in the early applications. The current improved version, based on validation studies using the St. Louis RAPS data base, includes improved initial conditions as well as the facility for lateral spread and background entrainment (Schere and Shreffler, 1982b). The ACTM (Reynolds et al, 1979) is also a vertically multi-layered trajectory model. Some other improvements in this model relative to the city-specific EKMA are as follows: dynamic reactive simulation is carried out in the aloft layers; downwind emissions (assumed as constant on county-wide average basis in EKMA) are variable spatially and temporally; ground removal by dry deposition is included for some species. Comparisons of predicted ozone concentrations for the UAM and the ACTM were found to be in good agreement along most of the trajectory

for both the CBM and the DS-PBM mechanisms in a simulation of the Los Angeles plume (Killus and Whitten, 1984).

In a comparison of the performance of the DS-PBM, the ERT-LPM, and the SAI-UAM based on 20 days of St. Louis RAPS data (Schere and Shreffler, 1982a; 1982b), some of the important conclusions were as follows:

- the PBM applies only for stagnant flow conditions, and peak ozone predictions tended to be generally somewhat on the high side;
- the modification of LPM to facilitate lateral expansion of the plume and background entrainment resulted in marked improvement of performance;
- while the UAM is a powerful tool with broad capabilities, agreement between observed and predicted values at specific points in space and time are often poor, even in relatively simple flow situations as in St. Louis. An error of only a few degrees in input wind direction can lead to gross errors in specific air quality predictions (even within a domain which hardly extends far downwind of the urban source complex). Such errors are common when standard objective techniques of wind interpolations are used based on the usual wind data base available for most cities. When not paired in time and space, model predictions of daily ozone peak within the computational domain were usually within 30% of the observed values.

An examination of existing models has revealed that there exists no trajectory model with crosswind resolution capable of accepting the detail of the available St. Louis emissions inventory, and of simulating the type of ozone profiles observed 200 km downwind of St. Louis from *in-situ* continuous aircraft measurements on 9 July 1976. Our model, described below, attempts to do that.

4. DESCRIPTION OF OUR MODEL

4.1 Overview

The motivation for the development of this model is based partly on the availability of two types of detailed spatially-resolved chemical data, at least for St. Louis. First is the detailed gridded RAPS emissions inventory of St. Louis, in which the grid size varies from squares of 1 km sides in the urban core progressively to squares of 10 km sides in the urban outskirts. The other data base is the *in-situ* plume ozone data, measured from airborne platforms up to 300 km downwind of complex source areas, and possessing sufficiently detailed crosswind resolution to depict persistent fingerprints of the spatial inhomogeneities in the horizontal distribution of the precursor emission field even at such long distances. The data of the St. Louis metropolitan plume for 9 July 1976 give ample evidence of the existence of two diverse components of the metropolitan plume in terms of ozone production, one part (urban) deriving the needed precursors from the primary emissions, and the other (Labadie) depending critically on the background to supply some key precursor reactants. Our model possesses arbitrary crosswind resolution, and explicitly facilitates plume-background, plume-aloft, and background-aloft interactions in a dynamic mode.

Model formulation is essentially hybrid (Lagrangian/Eulerian), and may best be described in terms of a semi-infinite vertical slab (infinite in the crosswind direction, of fixed thickness in the downwind direction, and of height equal to the peak mixing height of the day of simulation) moving along a Lagrangian trajectory with the prevailing wind, over the source region and down to the farthest downwind distance of simulation. Figure 3 illustrates some of the model features within such a context. The upper figure shows the time-height (t-z) cross-section of the volume swept by the slab from 0600 to 2100, and the lower figure shows a horizontal plane extending laterally over the width of a metropolitan plume emitted into the slab, as the plume expands during downwind transport between time t and $t + \Delta t$.

In the vertical plane, the model is resolved into two layers -- the mixing layer and the aloft layer. Each is well-mixed vertically. Each is modelled dynamically. The aloft layer composition changes by chemical reactions. The mixing layer background concentration of each modelled species changes due to vertical dilution with entrained air from aloft during mixing layer growth, as well as due to chemistry and ground removal by dry deposition.

In the crosswind direction (Figure 3, lower), the metropolitan plume within the moving slab is resolved into N pillars, all of the same vertical extent as that of the plume bulk. All species are assumed to be uniformly distributed within each pillar, but the crosswind concentration profile of any species j at time t, i.e. $C_j(t)$, is free to be arbitrarily inhomogeneous, and non-similar to that of any other species. The plume width, W_p, is discretized into the N segments at the time of initialization based on any rational scheme. The pillar widths can be arbitrarily non-uniform. Subsequently, as the plume expands, each pillar width expands in the same proportion as the overall plume width. Thus, when each individual pillar width is normalized with respect to the total plume width, a transformed moving crosswind grid, which is invariant with respect to time, results. An Eulerian-type mass continuity equation for each species in each plume pillar, in the aloft layer, and in the background, provides the basic mathematical formulation for the instantaneous rate of change of the species concentration fields. The processes incorporated into the plume equations include dilution and entrainment from aloft due to vertical expansion, dilution and entrainment/detrainment due to lateral pillar expansion, crosswind diffusion tending to smooth out concentration gradients, chemical reactions, and ground removal. Boundary conditions at plume edges explicitly facilitate the entrainment into the plume of background air.

Temporally, the aloft and background simulations are commenced early in the morning (0600). Metropolitan emissions are released into the background during some subsequent period. Also, regional emissions are

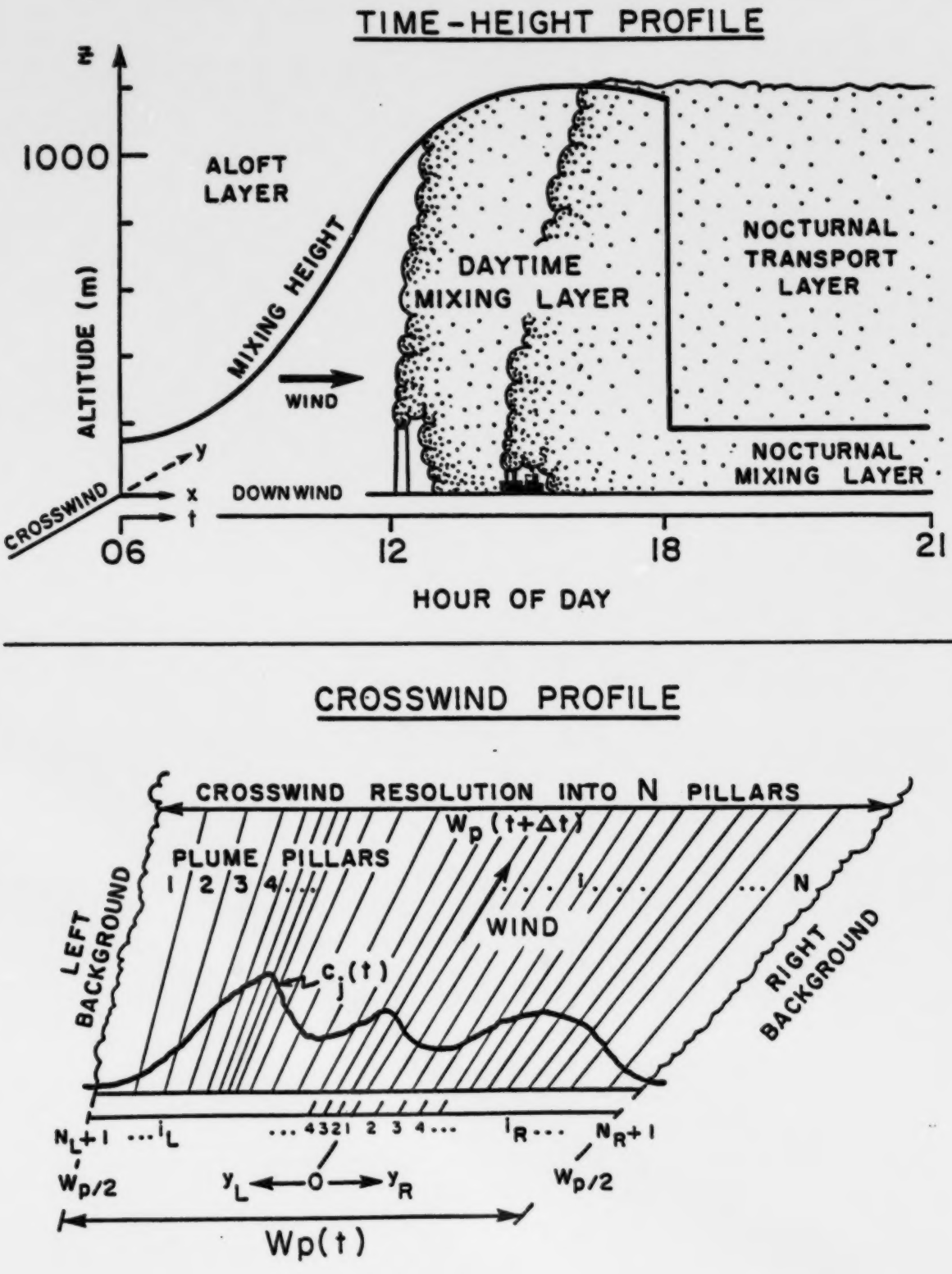

Figure 1. Illustration of the coordinate system and of some model features in the time-height (t-z) plane, and in the horizontal (t-y) plane between times t and t+ Δt.

released dynamically into all modelled entities in contact with the ground. At 1800 (for Midwestern summer), the mixing layer is assumed to collapse suddenly to its nocturnal shallow depth. The contents of the daytime mixing layer above the nocturnal mixing height are detrained into the nocturnal transport layer aloft which remains decoupled from ground removal effects. The remaining material flows into the surface-based nocturnal mixing layer, and continues to feel the effect of ground removal.

In the early version of the model presented here, only gas-phase chemistry is included based on an expanded form of the original DS-PBM mechanism which includes sulfur chemistry. This mechanism is consistent with the chemical resolution (four classes -- olefins, aromatics, paraffins, and aldehydes) of the available data of hydrocarbon emissions. It is recognized that this mechanism is now outdated and inaccurate in some respects. The preliminary results presented here must therefore be viewed with caution. They probably represent the upper limit ozone formation in the plumes. Future versions of the model will include more current and accurate mechanisms. Removal by dry deposition is parameterized in terms of the deposition velocity concept, and is included for SO_2, NO_2, O_3, PAN and H_2SO_4 only.

The model is intended to be diagnostic in that all meteorological variables are presumed to be measured inputs. Only the chemical variables, i.e. the species concentrations, are the subject of model calculations.

4.2 Mathematical Formulation

The hybrid formulation of the model splits the overall problem into two parts: a downwind component, and a cross-sectional component. The downwind component involves determination of the Lagrangian trajectory

of the plume, and the crosswind component involves an Eulerian formulation in the y-z plane.

The determination of the Lagrangian trajectory of any emission is based on a plume Monte Carlo simulation technique (White and Patterson, 1983). Input requirements include dynamic specification of the vertical plume transport layer and the wind data for this layer. The simulation is carried out in half-hour intervals. All wind vectors pertinent to each half-hour transport interval and the corresponding transport layer domain are pooled into individual data-sets. The primary emission is simulated by the release of many "dots" (100 in the present application) from the source into the initial transport layer domain. Each dot represents a fixed fraction of the emission mass. Each dot is then advected over the next half-hour based on a randomly selected wind vector out of the appropriate data set (wind vector pool for current half-hour interval). The procedure is repeated for all dots for successive time intervals as long as desired. The result is an expanding cluster of the dots, advancing downwind. The spread of the cluster is due to the variability of the wind field (both real and that resulting from measurement errors). As will be demonstrated in the section on model application, the trajectory as well as lateral plume spread predicted thus are in surprisingly excellent agreement with observed location and spread of the plume as far as 200 km from the source, given a well-defined wind field based on approximately 5 wind soundings per hour along the trajectory.

The Eulerian formulation involves the mass balance for each species in each cell of the moving vertical slab. The mass balance equations, expressed in terms of species concentrations, are summarized below.

4.2.1 Basic Equation for Plume Pillar i, Species j

$$\frac{\partial C_{ji}}{\partial t} = \left(\frac{\partial C_{ji}}{\partial t}\right)_{\text{emission}} + \left(\frac{\partial C_{ji}}{\partial t}\right)_{\substack{\text{vertical}\\ \text{dilution/}\\ \text{entrainment}}} + \left(\frac{\partial C_{ji}}{\partial t}\right)_{\text{lateral dilution}} + \left(\frac{\partial C_{ji}}{\partial t}\right)_{\substack{\text{lateral}\\ \text{entrainment/}\\ \text{detrainment}}} + \left(\frac{\partial C_{ji}}{\partial t}\right)_{\substack{\text{lateral}\\ \text{diffusion}}} + \left(\frac{\partial C_{ji}}{\partial t}\right)_{\text{chemistry}} + \left(\frac{\partial C_{ji}}{\partial t}\right)_{\substack{\text{dry}\\ \text{deposition}}} \qquad (1)$$

$$i = 1,2,3,\ldots,N \quad ; \quad j = 1,2,3,\ldots,N_{sp}$$

Details of each process term on the right side of the equation are given below.

In the present stage of model development, the source term (the first term in equation 1) includes the effect of regional surface emissions only. Primary emissions from metropolitan sources are treated by means of appropriate initial conditions. When major sources within the metropolitan plume are displaced in time, they are treated individually until their plumes line up along a common crosswind section. At that time, a new initialization is performed for the entire metropolitan plume. This method of treating primary anthropogenic emissions is viewed as the major shortcoming of the current version of the model. Future revisions will be aimed at including such emissions into the source term of the mass balance equations. Regional surface emissions are treated in the source term of the model equation as variable in time, but uniform spatially. They play a crucial role in the proper dynamic characterization of the background chemical composition, and in turn, of plume chemistry. Their role is carefully investigated in this paper.

$$\left(\frac{\partial C}{\partial t}_{ji} \right)_{\substack{\text{vertical} \\ \text{dilution/} \\ \text{entrainment}}} = -\frac{1}{H'} \frac{dH'}{dt} (C_{ji} - C^*) \quad , \tag{2}$$

where $H' = \begin{cases} H_P \ , & H_P < H_M \\ H_M \ , & H_P = H_M \end{cases}$ (H_P - plume height) (H_M - mixing height)

and $C^* = \begin{cases} C_{\text{Background}} \ , & H_P < H_M \\ C_{\text{Aloft}} & H_P = H_M \end{cases}$

This term becomes and remains zero after H_M reaches its peak value for the day.

$$\left(\frac{\partial C}{\partial t}_{ji} \right)_{\substack{\text{lateral} \\ \text{dilution}}} = -\frac{1}{W_P} \frac{dW_P}{dt} C_{ji} \quad , \tag{3}$$

$$\left(\frac{\partial C}{\partial t}_{ji} \right)_{\substack{\text{lateral} \\ \text{entrainment/} \\ \text{detrainment}}} = \left[\frac{\partial}{\partial y} \left(C_j \frac{dy}{dt} \right) \right]_{\text{cell } i}$$

$$= \frac{1}{W_P} \left[\frac{\partial}{\partial \eta} \left(C_j \frac{d(\eta W_P)}{dt} \right) \right]_{\text{cell } i} \quad , \tag{4a}$$

where $\eta_i = y_i / W_P$ is the transformed crosswind coordinate of the inner edge of cell i. This transformed coordinate is invariant in time. Therefore,

$$\frac{d\eta}{dt}_i = 0, \text{ and}$$

$$\left(\frac{\partial C}{\partial t} ji \right)_{\substack{\text{lateral} \\ \text{entrainment/} \\ \text{detrainment}}} - \frac{1}{W_p} \frac{dW_p}{dt} \left[\frac{\partial}{\partial \eta} \left(C_j \eta \right) \right]_{\text{cell } i} , \quad (4b)$$

$$\left(\frac{\partial C}{\partial t} ji \right)_{\substack{\text{lateral} \\ \text{diffusion}}} - \frac{\partial}{\partial y} \left(K_y \frac{\partial C}{\partial y} ji \right) - \left(K_y / W_p^2 \right) \cdot \frac{\partial^2 C}{\partial \eta^2} ji , \quad (5)$$

where K_y represents a mass exchange coefficient, or an "effective diffusion" coefficient incorporating the effects of both microscale turbulence and wind shear due to inhomogeneities in the mean wind field. Its magnitude is thus expected to be substantially greater than the usual K_y denoting just the turbulent diffusivity.

$$\left(\frac{\partial C}{\partial t} ji \right)_{\text{chemistry}} - \sum_P P_{ji} - \sum_R L_{ji} C_{ji} , \quad (6)$$

where the first summation represents the total production rate of species j from all chemical reactions in which it is produced, and the second summation represents the total depletion rate of species j from all reactions in which it is a reactant. In general, this is the most complex term of equations (1). It is the source of the non-linearity as well as the "stiffness" of the mass balance equations.

$$\left(\frac{\partial C}{\partial t} ji \right)_{\substack{\text{dry} \\ \text{deposition}}} - -k_{r_j} C_{ji} , \text{ where } k_{r_j} - v_{Dj} / H' \quad (7)$$

v_D denotes the deposition velocity. This term is only effective after plume touchdown. After the evening transition of the mixing layer, it operates only on the material in the shallow nocturnal mixing layer.

4.2.2 Basic Equations for Background and Aloft

$$\left(\frac{\partial C^j}{\partial t}\right)_{Bg} = \left(\frac{\partial C^{j,Bg}}{\partial t}\right)_{\substack{\text{vertical}\\ \text{dilution}}} + \left(\frac{\partial C^{j,Bg}}{\partial t}\right)_{\text{chemistry}}$$

$$+ \left(\frac{\partial C^{j,Bg}}{\partial t}\right)_{\substack{\text{dry}\\ \text{deposition}}} + \left(\frac{\partial C^{j,Bg}}{\partial t}\right)_{\substack{\text{regional}\\ \text{emission}}} , \qquad (8)$$

and

$$\left(\frac{\partial C^j}{\partial t}\right)_{Aloft} = \left(\frac{\partial C^{j,Aloft}}{\partial t}\right)_{\text{chemistry}} , \qquad (9)$$

$$j = 1,2,3,\ldots,N_{sp}$$

In the model, the left and the right background are treated as separate entities, in general. The background and aloft domains are infinite well-mixed reservoirs in the crosswind direction, and hence, there are no crosswind mass redistributions in them. Furthermore, aloft concentrations are also unaffected by vertical dilution or ground removal effects. The chemistry, however, is a ubiquitous process.

4.2.3 Initial and Boundary Conditions

Initial values of the concentrations of all species in all plume pillars, and in the aloft and the background, must be specified. The details of this step will be presented when model application is considered.

The background and the plume are bounded vertically at both ends of the boundary layer. The mass exchanges across the top and bottom boundaries are, however, included in the main model formulation (aloft entrainment and ground removal), and no boundary conditions are needed at those surfaces. In the crosswind direction, the plume boundary conditions are as follows:

$$\frac{dy}{dt} = 0 \quad \text{at plume centerline,} \qquad (10a)$$

and $C_j(y_L - W_P/2) = C_{Bg,\ Left}$

$$C_j(y_R - W_P/2) = C_{Bg,\ Right} \qquad (10b)$$

These boundary conditions refer to the coordinate system shown in Figure 3 (lower). $y_L = 0 = y_R$ represents the geographical midpoint between plume edges; $y_L = W_P/2$ and $y_R = W_P/2$ represent the left and right edges of the plume. The plume pillars expand and spread outwards from the vertical mid-plane. The mid-plane itself moves along the plume centerline trajectory, and by definition, there is no lateral mass entrainment/detrainment across this plane. There is no assumption of any type of symmetry of mass distribution about the mid-plane. It is also not required that the number of pillars on either side of the center plane be the same, since pillar widths are not required to be uniform.

In the model application, meteorological and plume physical variables are supplied as empirical inputs. These include $H_M(t)$, $H_P(t)$, $W_P(t)$, $K_y(t)$, and $R_T(t)$ = total solar radiation (used in the parameterization of the photochemical rate constants and the deposition velocities). In addition, the temporally invariant crosswind grid coordinates, η_i, of the plume must also be supplied initially.

4.3 The Chemical Scheme

In the current version of the model, an expanded form of the Demerjian-Schere chemical scheme is used. The original version involved 24 variable species and 36 reactions. These species are identified below:

O, O_3
OH, HO_2, H_2O_2
RO, R_2O, RO_2, R_1O_2, R_2O_2
NO, NO_2, NO_3, HONO, HNO_3, HO_2NO_2, $RONO_2$, PAN
CO, CO_2
OLE, ARO, PAR, ALD (Hydrocarbon classes)

Our expansion of this scheme first involves the addition of sulfur chemistry. This is achieved by the inclusion of the species SO_2 and H_2SO_4, and the reactions

37. $SO_2 + OH \rightarrow H_2SO_4 + HO_2$ $\quad k_{37} = 1.75\times10^3$ ppm^{-1}min^{-1}
38. $SO_2 + HO_2 \rightarrow H_2SO_4$ $\quad k_{38} = 1.30$ ppm^{-1}min^{-1}
39. $SO_2 + RO_2 \rightarrow H_2SO_4$ $\quad k_{39} = 0.78$ ppm^{-1}min^{-1}

Observe that in reaction 37, HO_2 is also a product. This is based on a recent suggestion by Stockwell and Calvert (1983). The production of HO_2 serves to recycle OH and to reduce the non-linearity of the sulfur chemistry. It also serves to counter ozone depletion by NO in fresh plumes, but provides a sink for ozone in aged plumes. The above rates of reactions 38 and 39 are now outdated. Current estimates for both are about 3 orders of magnitude smaller.

Another addition to the original DS-PBM chemistry is the photolysis reaction of H_2O_2, as follows:

40. $H_2O_2 \rightarrow 2OH$ $\quad k_{40} = k_{H_2O_2}^*$

The final scheme includes four photolysis reactions, for NO_2, HONO, aldehydes, and H_2O_2. The photolysis rates (k_j^*) for the last three of these are scaled with respect to $k_{NO_2}^*$ by the following factors

HONO : 0.1973

aldehydes : 0.002464

H_2O_2 : 0.003704

For photolysis rate for NO_2, we have formulated and used the following parameterization:

$$k_{NO_2}^* = C \cdot R_T \cdot \cos\theta_z, \qquad (11)$$

where C is a constant, R_T represents the total solar radiation in kW/m^2 measured at ground level, and θ_z is the solar zenith angle, calculated as follows:

$$\cos\theta_z = \sin\delta \sin\phi + \cos\delta \cos\phi \cos\omega,$$

where declination $\delta = 23.45 \sin(360 \times [284 + n]/365)$,
solar angle $\omega = -15(t - 12)$,
and ϕ, n, t represent respectively the latitude, the Julian date, and the hour of day.

The constant C is estimated based on data presented by Demerjian et al (1980) for $k_{NO_2}^*$. According to these data, the $k_{NO_2}^*$ value in St. Louis at noon on June 21 ($\theta_z \approx 15°$) under clear sky conditions ($R_T \approx 0.93$) may be expected to range between about 0.52 min^{-1} at ground level and 0.65 min^{-1} at a height of 1.2 km. Using an average value of 0.60 min^{-1} for the typical daytime plume transport layer, the value of C is derived as 0.67.

4.4 Dry Deposition

The deposition velocity is assumed to have the following diurnal variation with insolation:

$$v_D \text{ (cm/s)} = A + B \cdot R_T(kW/m^2). \qquad (12)$$

The constant A denotes the night-time value. The following values of A and B, inferred from average values of v_D in the published literature, are used in the model:

Species	(A, B)	v_D (daytime average*)
SO_2	(0.30, 1.50)	approx. 1.0 cm/s
H_2SO_4	(0, 0.20)	approx. 0.1 cm/s
NO_2	(0.04, 0.19)	approx. 0.1 cm/s
PAN	(0.08, 0.38)	approx. 0.2 cm/s
O_3	(0.23, 1.13)	approx. 0.7 cm/s
all other	(0, 0)	0

*For sunny summer day in St. Louis

4.5 Numerical Analysis

In general, the initial discretization of the plume width may be performed based on any rational scheme, and the pillar widths can take any set of non-uniform values. The only *a priori* constraint placed on the initial discretization is that the midpoint of the initial plume width be the edge between any two neighboring pillars. At all subsequent times, the trajectory of this plume centerline remains the plume centerline, and the pillars on either side (N_L to the left and N_R to the right, $N = N_L + N_R$, N_L not necessarily equal to N_R) spread outward from the centerline. Let $w_i(t)$ denote the instantaneous width of any pillar *i*. Then,

$$\frac{w_i(t)}{W_P(t)} - \frac{w_i(0)}{W_P(0)} - \text{constant}$$

must be satisfied. It also follows that

$$\frac{1}{w_i}\frac{dw_i}{dt} - \frac{1}{W_P}\frac{dW_P}{dt} - \lambda_y(t), \text{ say.}$$

or, during any Δt,

$$\frac{\Delta w_i}{w_i} - \frac{\Delta W_P}{W_P}$$

Each pillar width maintains a constant proportion to the overall plume width at all times, and expands at the same fractional rate as the whole plume. Also, any contiguous group of pillars, or a sub-plume, will maintain a constant proportion with respect to the overall plume. Equations 11 are based on the assumption that the flow field is uniform in the y-direction over the extent of the plume.

Pillar coordinates are η_{i_L} $(i_L = 1,2,\ldots,N_L)$ and η_{i_R} $(i_R = 1,2,\ldots,N_R)$, respectively, on either side of the centerline, and denote the location of the inner edges (nearest to the centerline) of pillar i on either side. Thus, $\eta_{1_L} = 0 = \eta_{1_R}$. The numerical formulation of the dispersion terms in this coordinate system is summarized in the equation below, where i stands generally for i_L or i_R.

$$\left[\frac{\partial}{\partial t} C_{ji}\right] = -\lambda_z (C_{ji} - C^*) - \lambda_y C_{ji} + \lambda_y \left[\frac{C_{j,i+1}\,\eta_{i+1} - C_{ji}\,\eta_i}{\eta_{i+1} - \eta_i}\right]$$

$$+ \frac{2K_y}{W_P^2}\left[\frac{\alpha_i C_{j,i-1} - \beta_i C_{ji} + \gamma_i C_{j,i-1}}{\eta_{i+1} - \eta_i}\right], \qquad (13)$$

where $\lambda_y(t) = \frac{1}{W_P}\frac{dW_P}{dt}$, $\lambda_z(t) = \frac{1}{H'}\frac{dH'}{dt}$,

$$\alpha_i = \frac{1}{\eta_{i+1} - \eta_{i-1}} \quad , \quad \gamma_i = \frac{1}{\eta_{i+2} - \eta_i}, \text{ and } \beta_i = \alpha_i + \gamma_i.$$

When $i_R = 1$ (right center pillar), η_{i-1} and $C_{j,i-1}$ are replaced by η_{2L} and $C_{j,1L}$;

when $i_R = N_R$ (rightmost pillar), η_{i+2} and $C_{j,i+1}$ are replaced by

$$\eta_{N_R+2} = \eta_{N_R+1} + \xi\,(\eta_{N_R+1} - \eta_{N_R}) \quad , \quad 1 \le \xi \le 2,$$

and $(C_{j,Bg})_R$. $\eta_{N_R+1} = 0.5$ at the outer edge of the plume. An analogous treatment applies for the boundary conditions of the left side pillars.

The factor ξ must be chosen from numerical experimentation to avoid either a false accumulation of mass in the outermost pillars (ξ too small), or a false depression of the role of the plume - background interactions (ξ too large).

The physical (dispersion) and chemical processes acting on the plume are characterized by quite diverse time scales. In general, plume

dispersion is a much slower process than many of the plume chemical reactions. This fact is utilized to improve computational efficiency by decoupling the integration time step for the chemical term (δt) from that of the remaining terms ($\Delta t = n\ \delta t$). Assuming that dispersion is not very significant during δt, we perform the integration of the chemical term over δt successively in each pillar as if the pillars are physically decoupled entities. Such integrations are repeated n times, following which the other terms are integrated over the larger Δt. The integration of the non-chemical terms is performed by a simple forward difference in time. Thus, for example,

$$C_{ji}\ (t + \Delta t) = C_{ji} + (\text{sum of non-chemical rate expressions}) \cdot \Delta t.$$

All concentration values in the right side are the current, chemically updated values.

Integration of the chemical term is, in principle, the most complex step. The chemical equations are non-linear, as well as very "stiff" (involving time scales ranging over several orders of magnitude). The chemical problem involves a set of non-linear equations of the form

$$\frac{\partial C}{\partial t}_{ji} = P_{ji} - L_{ji}\ C_{ji} \quad , \quad \begin{matrix} i = 1,2,3,\ldots,N \text{ pillars} \\ j = 1,2,3,\ldots,N_{sp} \text{ species} \end{matrix}$$

where P and L are, in general, non-linear functions of the species concentrations.

If $N = 20$ pillars and $N_{sp} = 25$ species, the set includes 500 simultaneous equations. The chemical time scale for species j in pillar i is given by

$$\tau_{ji} = 1/L_{ji} \quad ,$$

and may, in general, be quite variable in space and time. The use of standard integration schemes such as the Runge-Kutta method is not

practical in this case, because they would require, for all integrations over species, space and time, the use of a fixed time step which is smaller than the smallest time scale of the problem. The corresponding amount of computation would be prohibitive indeed. Methods such as that of Gear (1971) are specifically designed for stiff equations, and are much more efficient through automatic dynamic control of time step and error. Gear's method is also very accurate. However, for a set of 500 and more equations of this type, even Gear's method would involve extensive computations. Before the development of Gear's method, it was common in such problems to invoke steady state assumptions, according to which the time derivatives were set equal to zero, rendering the equations algebraic, and giving the solution

$$(C_{ji})_{eqm} = P_{ji}/L_{ji} \qquad (14)$$

The steady state assumption is poor except when $\tau_{ij} \ll \delta t$, a condition not universally satisfied. A procedure often applied in recent years is the so-called QSSA (Quasi-steady-state Approximation), in which certain species which react relatively fast are presumed to be in steady state at all times. Gear's method is then applied to the differential equations of the remaining slower reacting species. Such an approach not only reduces the size of the differential problem, but also allows the choice of significantly larger time steps of integration in the Gear solution. The result is a substantial gain in computational efficiency. However, this gain is at the expense of accuracy. There is no *a priori* method to estimate the accuracy of QSSA, and comparisons of QSSA and full Gear solutions have indicated marked discrepancies in the QSSA solutions (for example, Farrow and Edelson, 1974). Even fast species may not react at a fast enough rate in all pillars to satisfy the QSSA at all times. Steady state assumptions, if invoked, must be made only locally in space and time when justified.

Hesstvedt et al (1978) developed a modified QSSA in which they monitored the value of the chemical time scale, $\tau_j(t)$, for all species at all integration steps, and invoked the steady state assumption only

when the criterion $\tau < \delta t/10$ was satisfied, in which case the fractional error of QSSA is less than e^{-10}. For very slow reacting species ($\tau > 100\delta t$), the assumption that $(\partial C/\partial t)$ = constant is valid, leading to a simple analytical solution. Even for the intermediate species, other simplifying assumptions were shown to be valid, leading to analytical solutions in all classes of τ. It was also shown that such judicial use of QSSA also gave solutions whose accuracy was comparable to that of Gear. Hov (1983) further simplified the application of the justified QSSA. He showed that an iterative solution based on the simple expressions:

$$C_j(t + \delta t) = C_{j,eqm}(t) \quad \text{for } \tau \leq \delta t/2 \quad , \tag{15a}$$

$$\text{and } C_j(t + \delta t) = C_j(t) + \delta t \, [\, P_j(t) - L_j(t) \cdot C_j(t) \,] \quad \text{for } \tau > \delta t/2 \tag{15b}$$

still gave a high degree of accuracy (within 1-2% of Gear solution for all species for a two day simulation of the polluted atmosphere), while requiring substantially less computation than in Gear's method. Five iterations were found to be adequate, given an appropriate choice of the time step size. In the calculations presented in this report, very small integration time steps were used to ensure numerical accuracy. Numerical experiments will be carried out in the future to establish larger optimum values. We have adopted the modified QSSA method of Hov (equations 15) to solve the set of chemical equations.

5. TESTING OF MODULES

The two major modules of the model, *viz.* the lateral dispersion module and the chemical module, were tested separately for accuracy.

5.1 Crosswind Dispersion Module

The numerical formulation of the complete dispersion module is given by Equation 12. The test described below pertains to a plume transport scenario in which plume height (H_P) is assumed to remain constant over the simulated period of transport. Consequently $\lambda_z = 0$, and the vertical dilution term of Equation 13 drops out. The test, therefore, is of the crosswind dispersion simulation including the effects of plume expansion, entrainment/detrainment, and diffusion in the crosswind direction. Figure 4 (upper) shows the continuous and discretized crosswind distributions of the concentration field of an inert species at time t_0 after release from three vertical co-planar sources, all of 1 km height. The sources have equal strength, 10 kg/s each. One source is a vertical line source located over the point y = 13 km in the source plane; a second source is a vertical area source of crosswind width 2 km centered at y = 23 km; the third source is a 1 km high by 10 km wide vertical area source extending between the centerlines of the first two sources. The crosswind locations of the first two sources are shown in Figure 4 (upper). The emissions are uniformly distributed over the extent of each source.

The source emissions and their subsequent transport are assumed to be into a meteorologically steady state environment, characterized by mixing height H_M, mean horizontal wind speed U, and effective lateral diffusivity K_y. For such steady state conditions, analytical solutions exist for the concentration fields downwind of line and area sources. Also, superposition of such fields is valid. For a uniform line source of height $H = H_M$ and strength = Q_0, located at $y = y_s$ the solution is

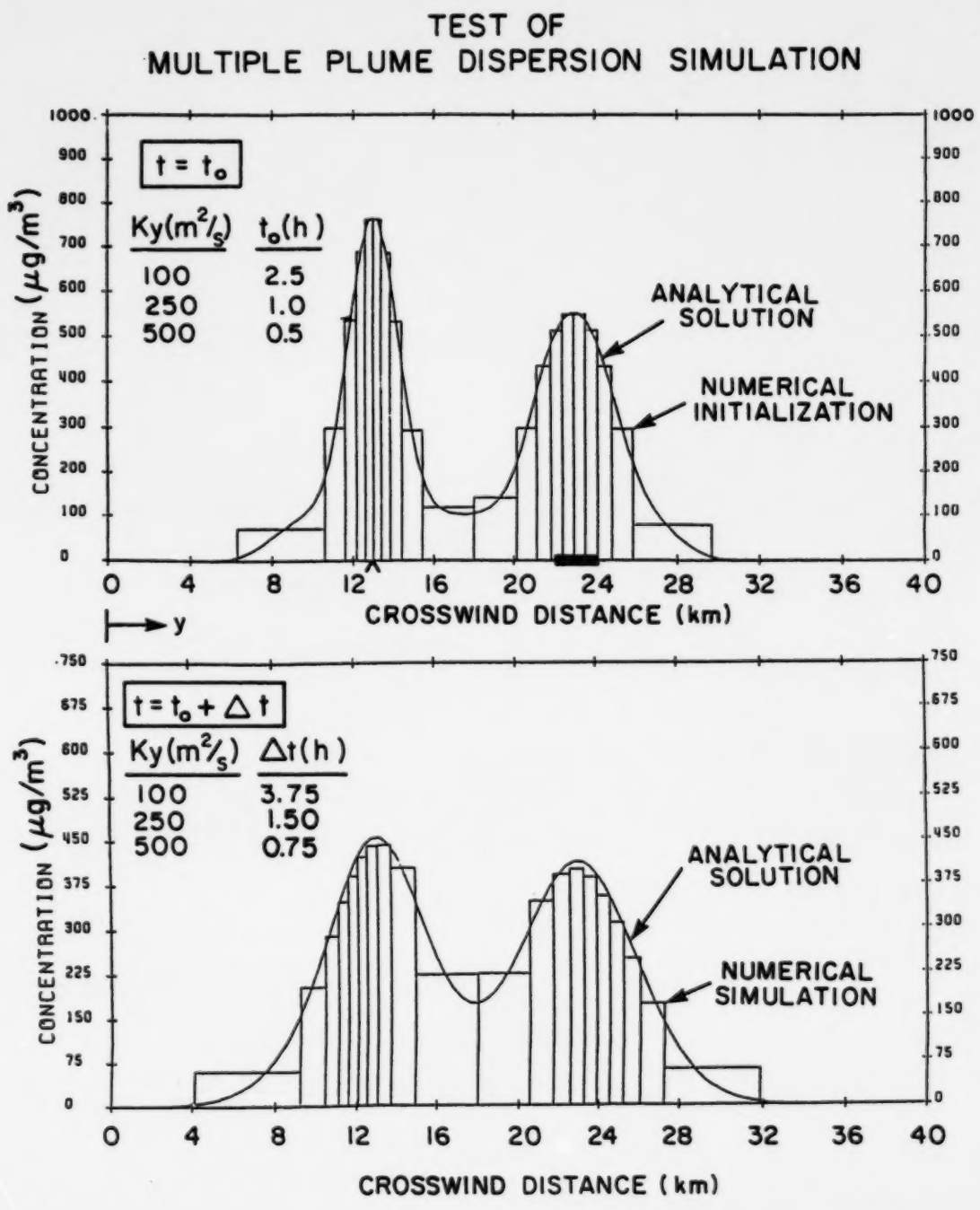

Figure 4. Test of numerical accuracy of the crosswind dispersion module for a scenario of known analytical solution for a complex 3-source release into a steady-state meteorological environment (H=1000 m, U = 5 m/s, K_y = constant, as indicated). The three uniform 1 km high sources have equal strength of 10 kg/s each, and are located at 13 km, 22-24 km, and 13-23 km.
(Upper) "Initial" condition when $\sigma_y^2(t_o) = 2\ K_y t_o = 1.8\ km^2$.
(Lower) Comparison of analytical and numerical solutions when $\sigma_y^2(t) = 2.5\sigma_y^2(t_o) = 4.5\ km^2$.

$$C(t,y) = \frac{(Q_0/UH)}{\sqrt{2}\ \sigma_y} e^{-\frac{1}{2}(y'/\sigma_y)^2} \quad , \quad \begin{matrix} -\infty < y' < \infty \\ t > 0 \end{matrix} \qquad (16)$$

where $y' = y - y_s$ and $\sigma_y^2 = 2K_y t$.

For a uniform area source of height H, width b and strength Q_0, centered at $y = y_s$, the solution is

$$C(t,y) = \frac{(Q_0/UH)}{4\ b} \left[\text{erf} \left(\frac{y' + b}{\sqrt{2}\ \sigma_y} \right) - \text{erf} \left(\frac{y' - b}{\sqrt{2}\ \sigma_y} \right) \right] \quad \begin{matrix} -\infty < y' < \infty \\ t > 0 \end{matrix} \qquad (17)$$

The continuous crosswind concentration profile shown in Figure 4 (upper) is the superposed analytical solution of the concentration field due to three given sources for $H_M = 1$ km, $U = 5$ m/s, and $\sigma_y = \sigma_y(t_0) = 1.342$ km. Thus, it is the solution, for example, at $t_0 = .5$, 1.0, or 2.5 h corresponding to $K_y = 500$, 250, or 100 m^2/s, respectively. The discrete initial solution is merely the redistribution of this mass into the grid pattern shown. The gridding scheme is chosen such that each grid cell contains an equal mass. There are 20 grid cells. This discretized concentration field is used as the initial condition which is subsequently dispersed in the given steady-state meteorological environment according to equation 13.

Figure 4 (lower) shows the analytical (continuous) solution of the concentration field when $\sigma_y^2(t) = 2.5\ \sigma_y^2(t_0)$, and the corresponding numerical (discrete) solution according to our model. Clearly, the numerical simulation is quite good. It was also verified that the accuracy of the numerical solution improved as the number of cells was increased, and became coarser as the number of cells was decreased.

5.2 Chemistry Module

The chemical module was tested in two ways. First, solutions were obtained by the Gear method and by Hov's modified QSSA method using the original Demerjian-Schere chemistry for a test smog chamber simulation scenario supplied by EPA. The two solutions closely matched each other for all species for the entire experimental period. They also matched the solution supplied by EPA. The second test was performed using another chemical mechanism -- the SCHEME surrogate mechanism developed by Levine and Schwartz (1983). The test included comparison of a Gear solution presented in that work for a particular chemical scenario (their Figure 3) with our solution for the same scenario using Hov's QSSA method. The agreement, once again, was excellent. In the application of the QSSA method, 5 iterations were performed at each time step.

6. MODEL APPLICATION

Model application is aimed at simulation of the observed crosswind profile of ozone for the 2000 traverse by the Washington University aircraft on 9 July 1976 (Figure 2 upper), approximately 150 km downwind of the St. Louis Gateway Arch and 190 km downwind of the Labadie power plant. At that location and time, the plumes of the Wood River petroleum refinery complex, the Sioux power plant, and the urban core region had merged into a broad plume about 50 km wide, with ozone concentration peaking in plume core at levels exceeding 100 ppb compared to a background level of about 63 ppb. The plume of the Labadie power plant was distinctly separate from the urban plume, with little evidence of significant interaction between the two plumes. The Labadie plume had a spread of about 30 km, and ozone in it peaked also over 100 ppb.

6.1 Plume Transport Simulation

Monte Carlo transport simulation of point source releases from an elevated source at Labadie at 1200 and a ground source at Wood River at 1500 are shown in Figure 5. These particular releases were selected from a number of trials corresponding to different release times from the two sources, based on their depiction of the likely physical history of the St. Louis plumes sampled in the 2000 traverse. Earlier releases were past section TT at 2000, while later releases fell short of TT at 2000. Full model simulation of the 1200 release of the Labadie plume was initialized at 1230 at the cross-section LL, and the metropolitan plume initialization was placed at 1530 at the cross-section MM. Labadie plume simulation was performed in two separate ways -- first as an isolated plume going from LL to the target receptor section (TT), and next as an isolated plume from LL to MM, and continuing as a re-initialized and more aged portion of the overall metro plume going from MM to TT.

The relative isolation of the Labadie plume presents an outstanding opportunity to characterize the meteorological variables, some of which are shown plotted in Figure 6. Solar radiation data are based on direct

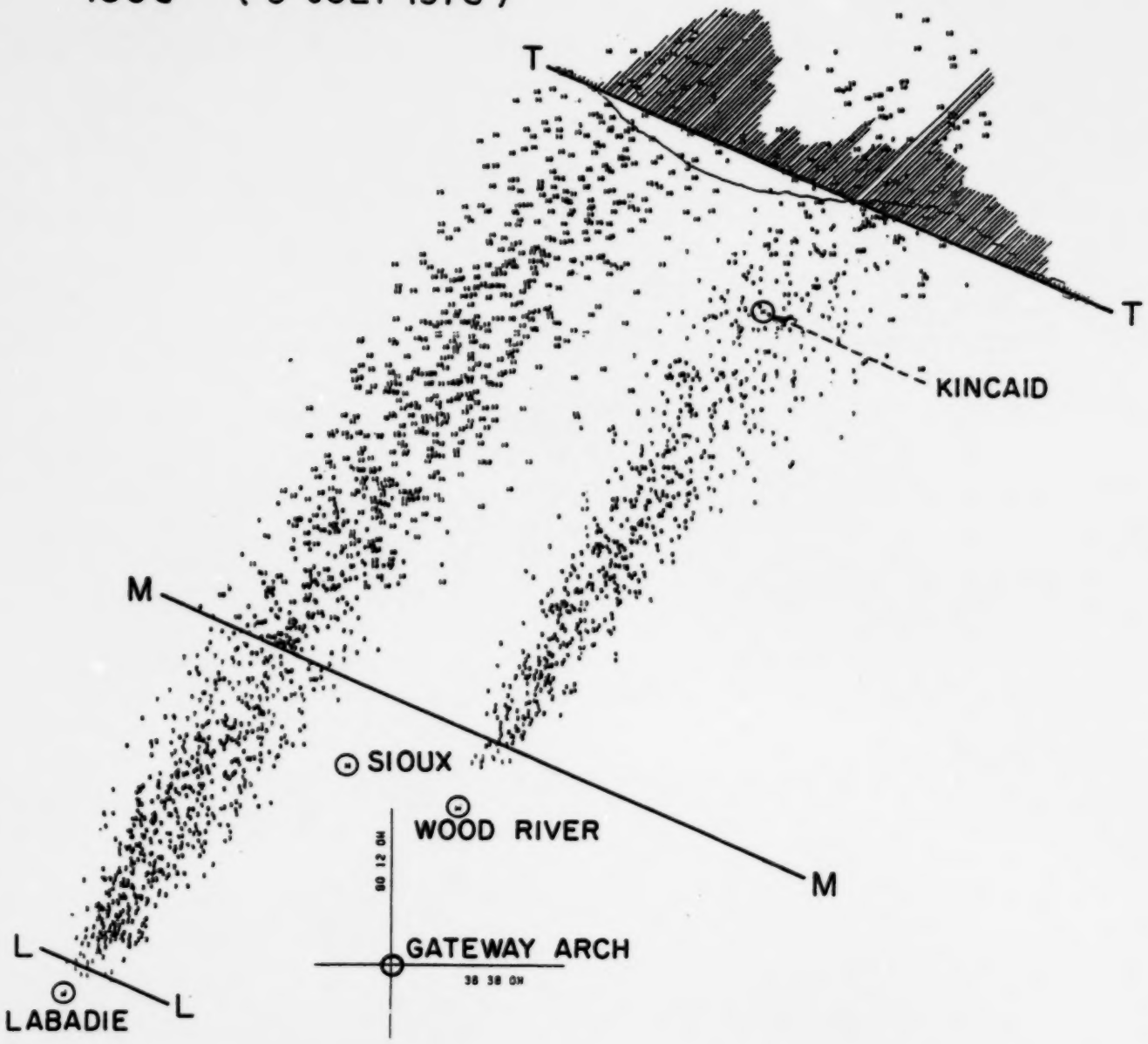

Figure 5. Monte Carlo transport of point releases from Labadie at 1200 and from Wood River at 1500 for 9 July 1976. Both releases arrive at section TT at about 2000. Observed concentration profile of SO_2 at 2000 aircraft traverse at TT is also shown. Observe that the simulated Labadie trajectory as well as spread are very well matched with the measured plume location and spread.

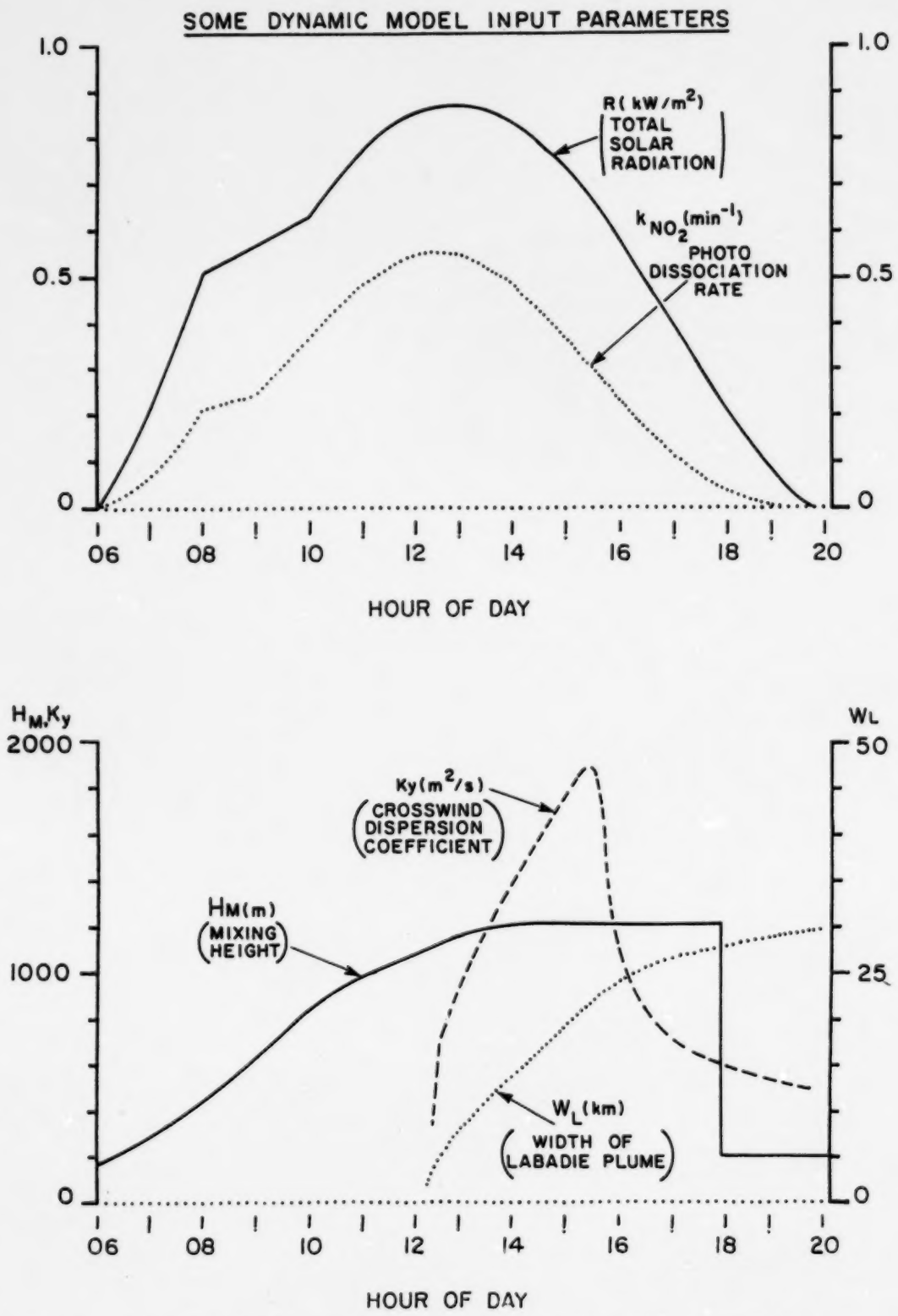

Figure 6. Some dynamic input variables of the model for 9 July 1986.

measurement at RAPS station 118 (a rural, relatively upwind station). Values of the NO_2 photo-dissociation rate are based on the parameterization formula (Equation 11). Daytime mixing height values were deduced from data of aircraft, wind, and temperature/humidity soundings (see Gillani 1978), and are believed to be quite reliable. The Monte Carlo trajectory of the Labadie plume not only arrives at the correct destination, but also shows a rather accurate spread of the plume. Fortuitous though this may be, it provides a very credible scenario for plume spread dynamics over the full trajectory. It is used as a guide in formulating the following analytical model of the width of the Labadie plume (W_L, also shown plotted in Figure 6):

$$W_L(t) = \begin{cases} 6t & , \quad t \leq 0.5 \\ 3 + 8(t - 0.5)^{0.8} & , \quad 0.5 \leq t \leq 3.5 \\ 22.3 + 4(t - 3.5)^{0.5} & , \quad 3.5 \leq t \leq 8.0 \end{cases} \qquad (18)$$

where plume width W_L is in kilometers, and transport time t is in hours. Based on this formulation, the widths of the 1200 release of the Labadie plume are 3 km at initialization (1230, section LL), 22.3 km at re-initialization for metro plume run (1530, MM), and 30.7 km at the target simulation traverse (2000, TT).

From the analytical expression of W, the quantities W, dW/dt, and $\lambda_y = 1/W\ (dW/dt)$ are easily evaluated at any simulation time. Also, $K_y(t)$ is estimated as follows:

$$K_y = \frac{1}{2}\frac{d}{dt}(\sigma_y^2) = \frac{1}{2}\frac{d}{dt}\left[\frac{W^2}{a^2}\right] \quad , \quad W = a\sigma_y .$$

Therefore, $$K_y(t) = \frac{1}{a^2} W \frac{dW}{dt} \qquad (19)$$

K_y is evaluated using $W = 4\sigma_y$ for the Labadie plume, and is shown plotted in Figure 6. The reader is reminded that K_y includes the dispersive effects of microscale turbulence as well as inhomogeneities in the mean wind field. The observed Labadie plume spread is used as a means to estimate the temporal behavior of K_y. The result (K_y), however, is of more general validity, and is used also in the metro plume run to estimate gradient smoothing in the entire metro plume by way of the diffusion term.

The width of the urban plume (including Sioux) at the time of initialization of the metro run (1530) is determined from the observed proportions of the urban and Labadie plumes at the 2000 traverse (respectively about 50 km and 30 km) and the previously estimated width of the Labadie plume at 1530. Thus,

$$W_{U,1530} = \frac{W_{U,2000}}{W_{L,2000}} \times W_{L,1530} = 36.2 \text{ km},$$

where the subscript U refers to the urban plume. The width of the Sioux plume is estimated to be about 7 km and of the remainder of the urban plume as about 29 km at 1530. Thus, the two power plant plumes together approximate half of the total width of the metropolitan plume. This estimate is also consistent with the observation in the 1600 aircraft traverse (Figure 2).

6.2 Characterization of the Ambient Environment

Proper characterization of the ambient environment is of crucial importance, particularly for power plant plume chemistry. While the importance to plume chemistry of the regional background both within and above the mixing layer is generally recognized, the subject has received inadequate attention in quantitative research. The sensitivity of power plant plume chemistry to background precursor concentrations (NOx, NMHC) is a major focus in this study.

Perhaps one reason for the relative neglect of background chemistry is the dearth of corresponding chemical data, particularly of the precursors. There is probably more available rural data for secondary species such as ozone and sulfates than for precursor hydrocarbons. Also, rural levels of NOx are usually close to the detection limits of most NOx monitors, and are therefore not reliably measured. The data base for important intermediate gaseous species such as OH, HO_2, RO_2 and H_2O_2 is even more scarce. Partly as a result of the lack of availability or reliability of background HC and NOx data, background ozone has occasionally been used in the past as a surrogate measure of background reactivity (Gillani et al, 1981). Also, model simulations of plume chemistry are characterized by widely varying assumptions concerning the input values of these precursors. Consider the following example pertaining to two separate model simulations aimed at the same field observations of ozone generation in the plume of the Oak Creek power plant (near Milwaukee, WI) during its midday transport over Lake Michigan on 20 July 1977 (Miller et al, 1978). No measurements were made of the hydrocarbons. In their model runs, Miller et al (1978) assumed midday background concentrations of NMHC to be 120 ppbv (approximately 480 ppbC) in comparison with a value of 200 ppbC used by Stewart and Liu (1981). Miller et al assumed a value of 30 for the ratio NMHC/NOx (in ppbv/ppbv), based on other measurements in the same area. Stewart and Liu used background NOx in the range 15-20 ppb, yielding NMHC/NOx value about an order of magnitude smaller than 30. Yet, both simulations were able to match closely the observed ozone in the background and in the plume at all three downwind aircraft traverses. Evidently, there were significant other differences in the model inputs of the two simulations. Unfortunately, as is the case frequently, little information is given by the authors concerning other input information, particularly concerning the background.

Hov and Isaksen (1981) and Fishman et al (1985) attempted to estimate the regional background air quality by a different, more objective, approach. They tried to characterize the precursor levels in the regional ambient environment by way of appropriate regional emissions of the precursors. It is estimated, for example, that the

northern hemispheric emissions of NOx averaged over the land surface are about 5×10^{10} molecules cm^{-2} s^{-1}; the corresponding values for eastern United States (EUS) and for the Northeast Corridor are estimated at about 2×10^{11} and 5×10^{11} molecules cm^{-2} s^{-1}, respectively (Clark, 1980). Fishman et al (1985) use a value of 2.5×10^{11} molecules cm^{-2} s^{-1} for average surface NO emissions over the eastern United States. There is greater uncertainty about the hydrocarbon emissions, since natural sources are also significant. Clark (1980) estimated anthropogenic NMHC/NOx emission ratio for EUS in 1977 as 1.15 by weight. Since about half of the NOx emissions are from point sources, the NMHC/NOx emission ratio for EUS anthropogenic area sources may be estimated to be about 2.3. Based on boundary layer model simulations, Hov and Isaksen (1981) found that third-day daytime ozone levels ranged between about 50 and 170 ppb for NOx regional emission rates ranging from 1×10^{11} to 5×10^{11} molecules cm^{-2} s^{-1}, respectively, with a constant NMHC/NOx emission ratio of 2. These results imply that average regional NOx emission rate of around 2×10^{11} molecules cm^{-2} s^{-1}, and NMHC/NOx emission ratio of about 2 may be appropriate for the observed ozone yield in the ambient environment of the St. Louis region.

We examined a particularly relevant and reliable recent data base of ambient hydrocarbon measurements at upwind, downtown, and downwind stations in the Columbus, OH area over a one month summer period. The rural stations were about 50 km from the downtown station. The results, summarized in Figure 7, show the corresponding spatial-temporal variation of NMHC. Most of the upwind levels of NMHC were close to 100 ppbC, and there was some tendency for decrease with the growth of the mixing layer. The figure also shows the average composition of urban NMHC measurements in different cities. The ambient data of NMHC and NOx for 9 July 1976 at the rural upwind RAPS stations were, unfortunately, not reliable and consistent.

Figure 8 shows our model simulations of the kinetics of the aloft and the mixing layers corresponding to the meteorological conditions of 9 July 1976. This simulation is termed the "standard run." The initial conditions used at 0600 are summarized in Table 1. The regional

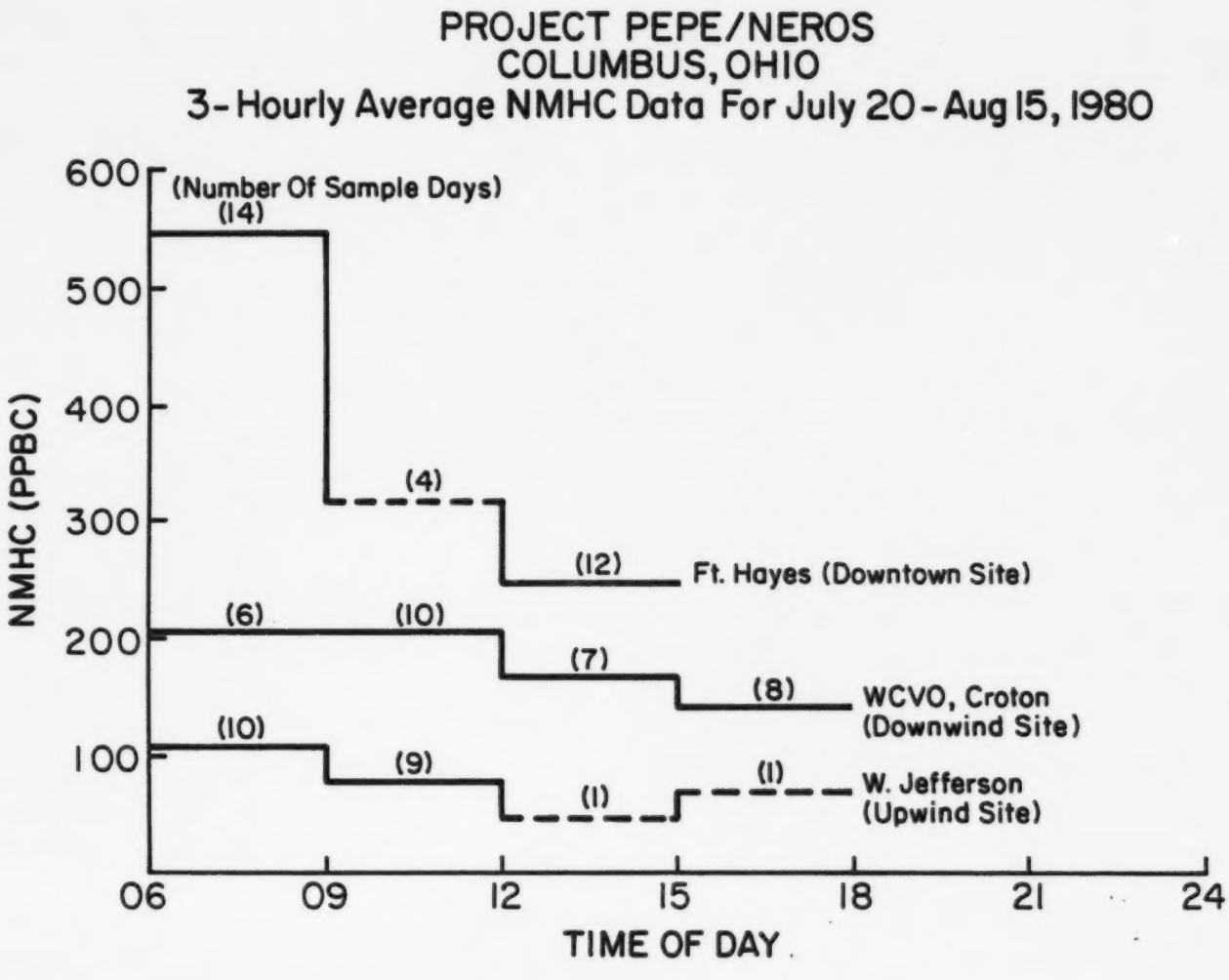

Figure 7. Spatial-temporal variation of ambient NMHC in the vicinity of Columbus, OH based on measurements of Project PEPE/NEROS.

emissions were varied somewhat to obtain a match of simulated and observed ozone simulataneously in the aloft and mixing layer backgrounds. Final values used in the standard run simulation are summarized below.

NOx (as NO): 3×10^{11} molecules cm^{-2} s^{-1} , 0600 – 1300
2×10^{11} molecules cm^{-2} s^{-1} , after 1300.
NMHC/NOx : 2 ppbv/ppbv , at all times.
NMHC composition: 60% paraffins (by volume)
25% aromatics (by volume)
15% olefins (by volume).

Such a regional emission contributes about 2 ppb/h of NO to the ambient concentration in the shallow mixing layer during 0600 – 0700, and about an order of magnitude less after 1300. For NMHC, the values are about twice as much.

The model calculations corresponding to the given choice of initial conditions and regional emissions give an excellent dynamic simulation of the observed ozone at all times except late in the evening. The NMHC concentration during the period of 0600 – 0900 generally remains higher than that observed in the upwind data of Columbus, OH (however, their participation in any chemistry is very weak during this period); for the 0900 – 1200 period, the match is close, and the levels during the afternoon appear to be lower than for Columbus. The discrepancy between observed and simulated ozone after sunset may be partly related to an inadequate treatment of night-time chemistry in the chosen chemical scheme.

Three important questions concerning daytime ozone dynamics in the mixing layer need to be addressed. They are:

1) How sensitive is mixing layer ozone to entrainment from aloft?
2) How sensitive is mixing layer ozone to the regional emission of NOx and NMHC?
3) How sensitive is plume ozone to the ambient air composition?

Table 1

AMBIENT INITIAL CONCENTRATIONS OF TRACE SPECIES AT 0600

SPECIES	CONCENTRATION (ppbv)	
	Mixing Layer	Aloft
SO_2	1.0	0
H_2SO_4	1.5	0
NOx (NO, NO_2)	6.5 (3.0, 3.5)	3.1 (0.1, 3.0)
HONO	0.625*	0.086*
$HONO_2$	2.0	0
PAN	0.7	0
NMHC (Par, Aro, Ole)	50 (31.5, 11.5, 7.0)	20 (16, 3, 1)
NMHC/NOx	7.7	6.5
Aldehydes	1.5	10.0
CO	500	250
H_2O_2	0	6.0
O_3	25	36
All other trace species	0	0

*Equilibrium concentration based on

$$NO + NO_2 + H_2O \overset{K}{\leftrightarrows} 2\ HONO$$

(H_2O concentration calculated from hourly RAPS data of T, RH).

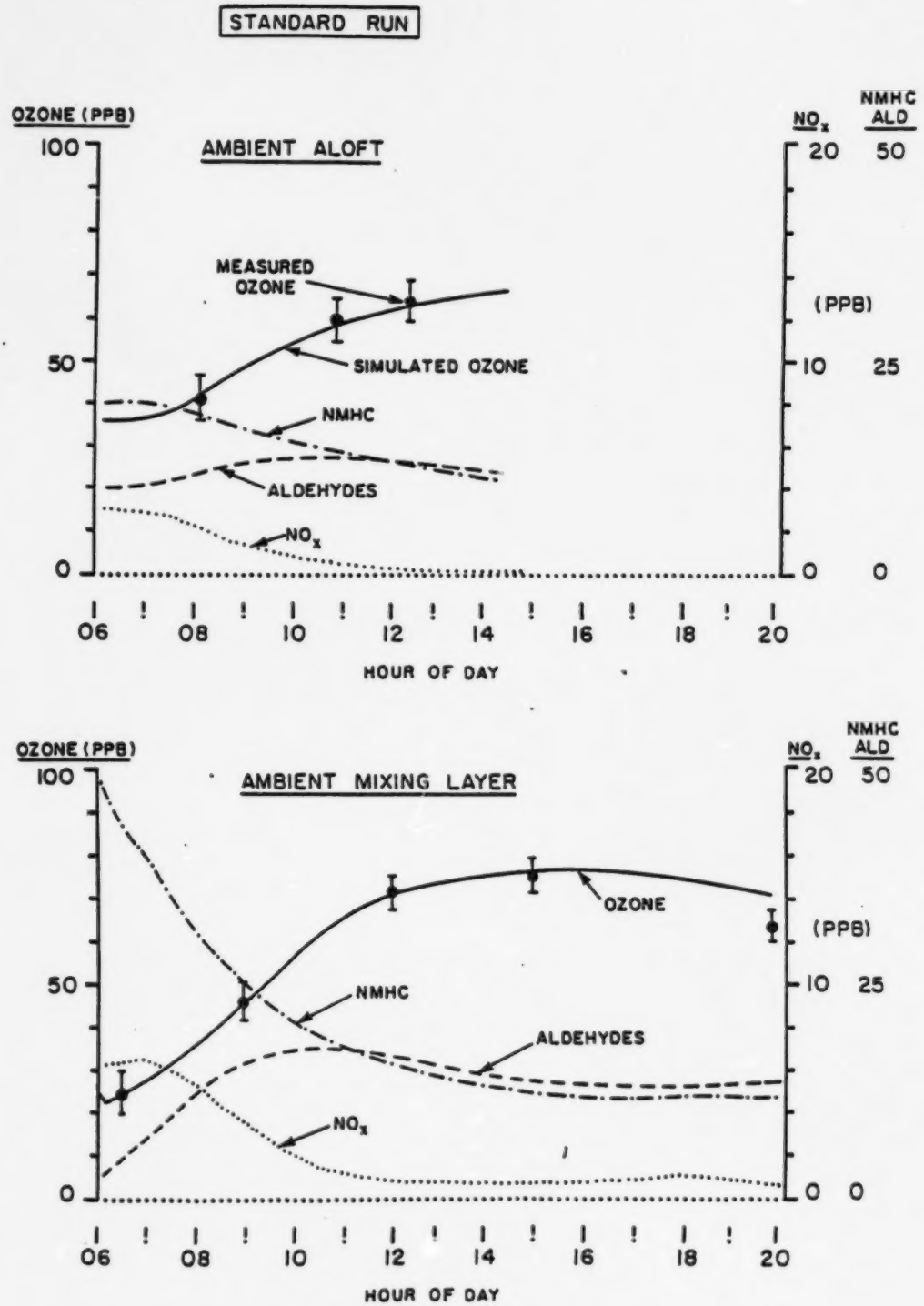

Figure 8. Standard run model simulation of the precursors and of ozone in the ambient airmass of 9 July 1976 near St. Louis. Measured ozone data are also shown. Measured data are from WU aircraft with one exception. The early morning (0600-0700) mixing layer value is based on ground level measurement at RAPS station 118.

The influence of error in the choice of the initial conditions of the precursor levels at 0600 is relatively small, because it is quickly diluted as the mixing layer grows from 150 m to over 1000 m rather rapidly in the morning.

Figure 9 shows a comparison of mixing layer ozone evolution during the day with and without the influence of a realistic aloft composition. It is clear that the influence of entrainment from the dynamic aloft layer plays a dominant role in shaping the observed behavior of mixing layer ozone in the morning. Before 1000, in particular, without the enrichment from aloft entrainment, there would be a net sink of ozone in the mixing layer due to the effects of vertical dilution, and of depletion by reaction with NO and by ground removal. This, however, is not the case in fact.

Figure 10 demonstrates the sensitivity of mixing layer background ozone to the choice of regional emission levels of the precursors. Curves (a) correspond to the standard run, with standard NOx surface flux ranging from (3 to 2)$\times 10^{11}$ molecules cm^{-2} s^{-1}, and NMHC/NOx flux ratio of 2. Curves (b) correspond to a four-fold higher NOx regional emission flux than the standard case, with NMHC flux being maintained at the standard level. Thus, NMHC/NOx flux ratio is 0.5 for this case. Initially (up to 1000), the increased NOx has a net effect of depleting ozone, but when the potential for photochemistry increases with insolation, the increased NOx plays a strong role in significantly enhancing net ozone generation. Curves (c) correspond to the case of a four-fold increase in NMHC regional emissions compared to the standard case, with NOx emissions maintained at the standard level. Thus, NMHC/NOx flux ratio is 8 for this case. There is only a small increase in net ozone production compared to the standard case. This increase is within the error range of measured ozone. The conclusion is that ozone production in the ambient environment is NOx-limited and not NMHC-limited. In general, the dynamic value of ambient NMHC/NOx concentration ratio (ppbv/ppbv) remains approximately at or above 8 for scenarios (a) and (c), for which ozone production is NOx-limited. This conclusion is consistent with observations based on laboratory

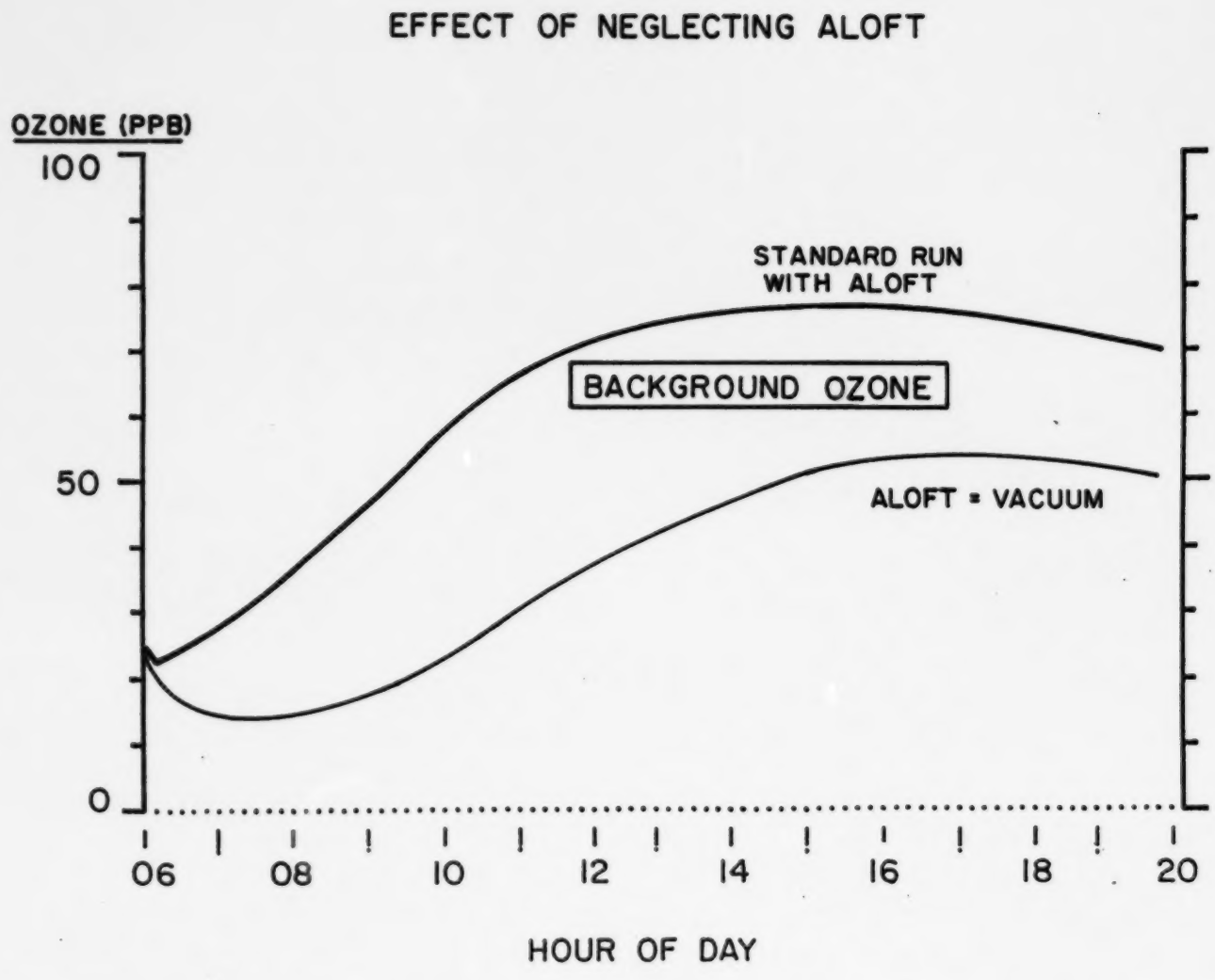

Figure 9. Influence of entrainment from aloft on ambient ozone in the mixing layer. The two curves are for a realistic scenario (standard run case) of the aloft air composition, and an unrealistic scenario (aloft = vacuum).

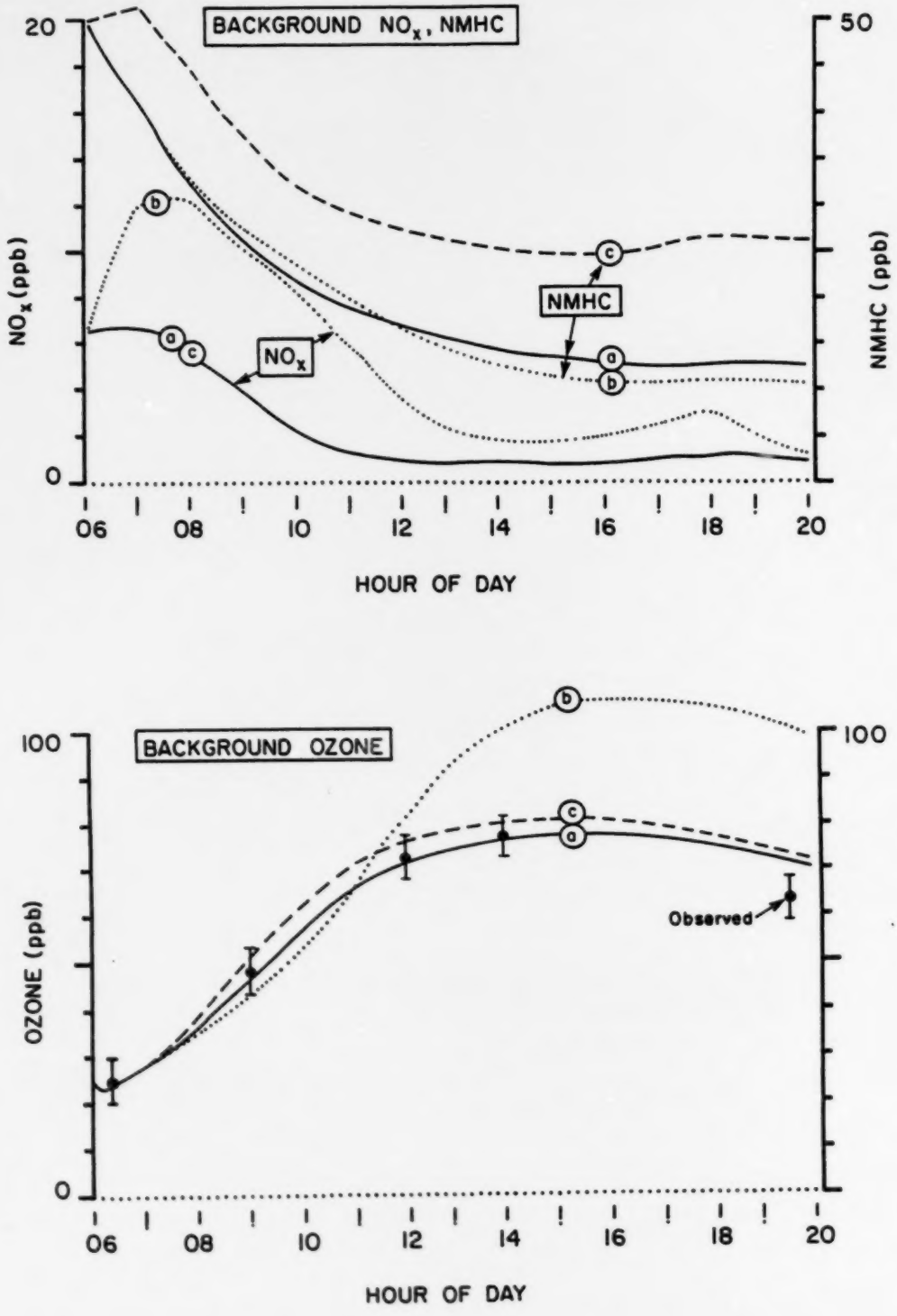

Figure 10. Sensitivity of background ozone in the mixing layer to regional emission flux of the precursors. Case (a) is same as the standard run $[(NMHC/NOx)_{Flux} = 2.0]$. Case (b) has 4 times higher NO_x flux $[(NMHC/NOx)_{Flux} = 0.5]$. Case (c) has 4 times higher NMHC flux than standard case $[(NMHC/NO_x)_{Flux} = 8.0]$.

experiments (for example, Dimitriades, 1978; Miller et al, 1978). Laboratory data also indicate that for mixtures of NMHC/NOx initial concentration ratio less than about 5.6, as is typically the case for both power plant and urban emissions, the limitation to ozone may be expected to be due mainly to NMHC. Thus, proper simulation of background ozone requires critically a proper input of ambient NOx levels, but a proper simulation of plume ozone generation may require a correct input of background NMHC also.

Our sensitivity analysis thus indicates that our choice of initial conditions and of the "standard" regional emission rate of NOx are appropriate for ambient ozone characterization, but for proper simulation of plume ozone as well, we need to investigate the sensitivity of plume photochemistry to ambient NMHC, in particular.

6.3 Sensitivity of Power Plant Plume Ozone to Ambient Air Composition

As we have seen, the ambient environment near St. Louis on 9 July 1976 (representative of summertime Midwestern United States conditions) was NOx-limited in terms of ozone production. It is reasonable, therefore, that injection of NOx from a power plant into such an environment leads to net ozone production in excess of ambient levels. However, since the power plant emission is itself characterized by very low NMHC/NOx initially, plume ozone generation must be NMHC-limited. Since the only source of NMHC in an isolated power plant plume is the background, proper characterization of background NMHC is important to plume chemistry. We therefore use the observed ozone chemistry in the Labadie plume as a means to explore and characterize background NMHC. For this purpose, we assume that the Labadie plume transport of 9 July 1976 was isolated from urban influence, and simulate the dynamics and kinetics of the 1200 release from Labadie within a spatially uniform, but temporally varying, background.

Primary emissions from Labadie on 9 July 1976 were well characterized on an hourly basis. Plant operations data provided estimates of rate of fuel (coal) burned around 1200, and the sulfur

content of that batch of fuel (about 3%). The SO_2 emission rate was thus estimated to be about 13 kg/s. Based on *in-situ* plume measurements at short downwind range, it was known that NOx/SO_2 in the plume is about 0.3 (by volume). Hence, the NOx emission rate (assumed to be 95% as NO and 5% as NO_2) was estimated as 1.88 kg/s. CO emission rate was estimated as 0.4% of the SO_2 emission rate (by mass).

The Labadie plume primary emissions of SO_2, NOx and CO were assumed to be distributed in a Gaussian form laterally, and uniformly in the vertical layer between 300 m and 900 m at initialization (1230). The crosswind plume spread of 3 km at that time was discretized into 10 pillars based on equal primary mass distribution. Hence there were 5 pillars on either side of the centerline, and the pillars became wider from plume core to edge in inverse proportion to the concentrations of the primary species. Initial concentrations for all other species in the plume pillars were determined as follows (using background values for 1230 from the previously described background simulation runs):

- NO, NO_2, O_3 based on the assumption of photostationary equilibrium, in the manner described by White (1977), requiring as inputs the NOx concentrations in the pillars and the NO_2 and O_3 concentrations in the background;
- HONO, H_2O_2 based on assumption of steady state equilibrium;
- all free radical species (χ) and O based on scaling with ozone, as $\chi_i/\chi_{Bg} = (O_3)_i/(O_3)_{Bg}$;
- all other species were assigned their background values.

Figure 11 shows the simulation results in the form of evolving crosswind profiles of ozone. The three separate cases shown correspond to cases a, b and c of the different regional emissions (a = standard NOx, NMHC; b = 4 × standard NOx; c = 4 × standard NMHC). In each case, the observed ozone profile at 2000 is also included for purposes of comparison and performance evaluation. Case (b) clearly represents a poor simulation, because plume ozone never even manages to catch up with the excessive ozone generation in the background. Of the cases (a) and (c) which both gave good simulation of the background, it

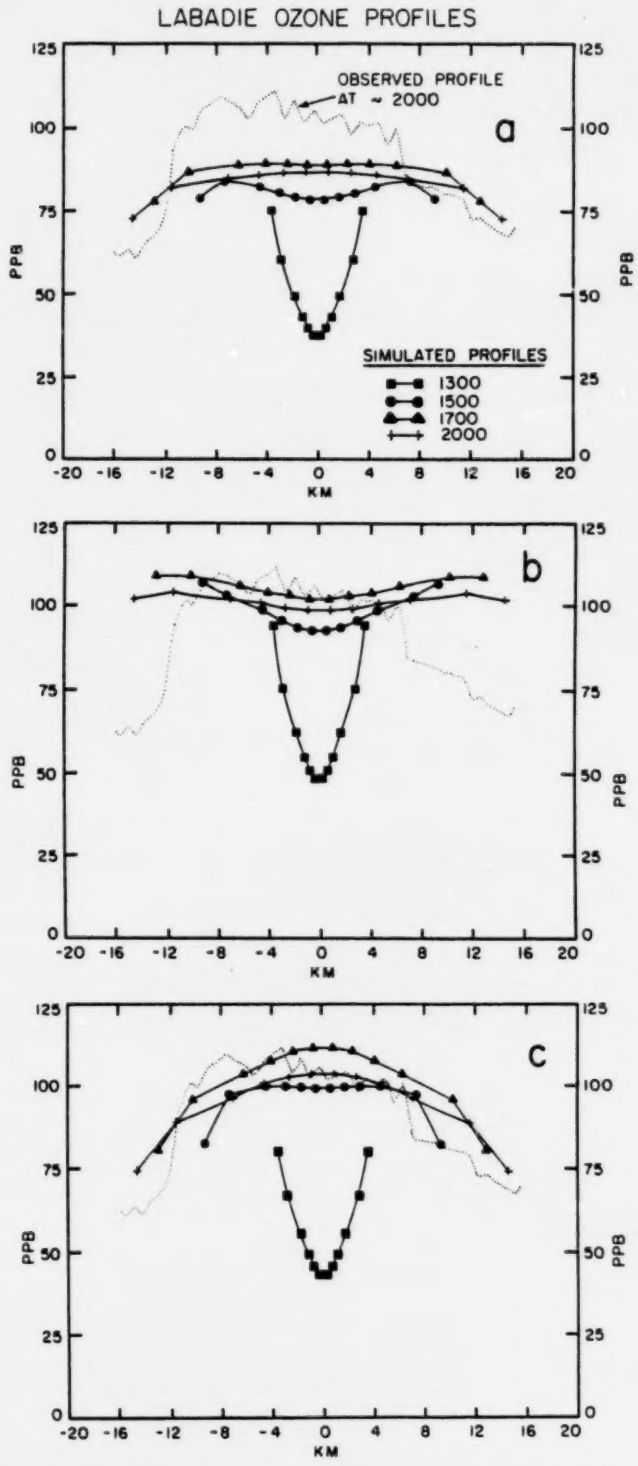

Figure 11. Evolution of simulated crosswind profiles of the Labadie power plant plume for 9 July 1976, corresponding to the three different cases of regional emissions of NOx and NMHC. Also shown in each plot is the observed ozone profile in the 2000 aircraft traverse. Case (c) represents the best overall simulation. (Symbol locations on each crosswind profile are placed at pillar centers. Observe that the core pillars are wider than pillars near plume edges. The ozone values at the outermost points of each profile denote the corresponding background value.)

is clear that case (c) represents a significantly better simulation of ozone within the plume. The simulation of case (c) is, in fact, in quite qood agreement with the observed profile of ozone. It follows, therefore, that based on the chemical scheme used in the model calculations, a good characterization of the ambient as well as plume chemistry is obtained using regional emissions as follows:

$$NOx = \text{standard case}$$
$$NMHC/NOx = 8 = 4 \times \text{standard case}.$$

The simulations (a) and (c) in which plume ozone generation is in excess of background levels also succeed in capturing the observed crosswind details depicting the three stages of chemical evolution of the plume. The early stage shows an ozone deficit; an intermediate stage shows the edge effect with more rapid ozone recovery on plume edges than in plume core; and the mature stages show the ozone bulge across the full plume cross-section.

Figure 12 shows the simulated dynamics of averaged values of plume ozone for cases a, b, c in comparison with the corresponding background level. It is evident that net excess ozone generation in the plume (cases a and c) is positively related to the level of background NMHC, and to the ratio NMHC/NOx in the background air. Examination of the plume NOx and NMHC levels at the time of complete recovery of the ozone deficit, and the onset of net excess ozone generation, show that the corresponding value of the ratio NMHC/NOx is about 1 (ppbv/ppbv), on a cross-sectionally averaged basis.

6.4 Sensitivity of Ambient and Plume Sulfur Chemistry to Ambient Air Composition

In the chemistry of photochemical smog formation, including the production of O_3, H_2SO_4, HNO_3 and PAN, the role of the free radical species OH, HO_2 and RO_2 is very important. OH is instrumental in the breakdown of the hydrocarbons (thereby generating HO_2 and RO_2), and in the oxidation of SO_2 and NO_2. HO_2 and RO_2 are principally responsible,

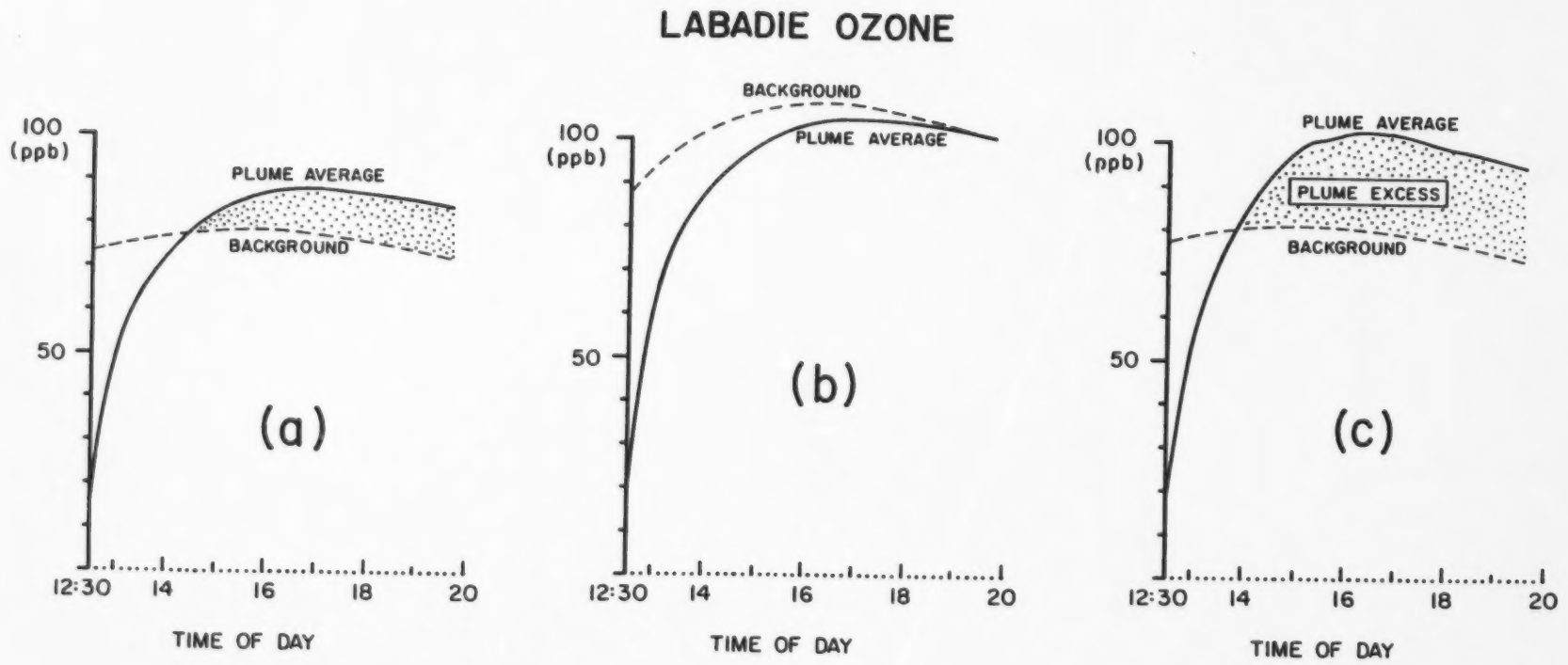

Figure 12. Dynamics of plume-average ozone in the Labadie plume of 9 July 1976 corresponding to the three cases of regional emissions of NOx and NMHC. The values of (NMHC/NOx) in the regional emissions fluxes for the three cases are a) 2.0, b) 0.5, c) 8.0. Excess plume ozone formation is positively related to the regional precursor flux ratio.

along with ozone, for the oxidation of NO to NO_2, and subsequent ozone production upon photolysis of NO_2. Figure 13 shows the plume average behavior of OH and HO_2 for the aloft air, for the mixing layer background, and for the Labadie plume, corresponding to cases a,b,c of regional emissions. The behavior of RO_2 is qualitatively very similar to that of HO_2, and its concentration levels are generally somewhat lower. Also shown in these plots is the behavior of H_2O_2, which is not only an important initiator of OH, but is also believed to be the principal agent for oxidation of SO_2 in the liquid phase. As such, it represents an important link between gas- and liquid-phase chemistry of sulfur.

The plot for the background shows that increased regional emission of NOx leads to increased production of OH (b), while an increase of NMHC (c) leads to increased production of the peroxy radicals (HO_2, RO_2). The effect of ambient NOx and NMHC on plume OH and HO_2 is exactly the opposite. Thus, the rate of SO_2 oxidation (dominated by reaction with OH) decreases in the background as the ratio NMHC/NOx of the ambient air increases (Figure 14), but increases in the plume. Thus, ozone as well as sulfate formation in power plant plumes correlate well with ambient NMHC/NOx in the polluted atmosphere characteristic of the eastern United States, but ambient ozone is not well correlated with ambient NMHC/NOx (being more NOx-limited). It follows that in a parameterization of power plant plume sulfur chemistry, use of ambient NMHC/NOx as a measure of the influence of the background ought to be more appropriate than using ambient ozone, as was done by Gillani et al (1981).

Examination of Figure 14 shows that for case (c), SO_2 oxidation rate in the Labadie plume briefly exceeded the ambient rate. The values of the rate for case (c) are, however, somewhat higher than those observed for the Labadie transport of 9 July 1976 (Gillani et al, 1978), even when the contributions of oxidation by the peroxy radicals are neglected. Simulation (c) thus compares well with field observations of ozone formation in the Labadie plume, but is somewhat disappointing with respect to sulfate formation in the plume.

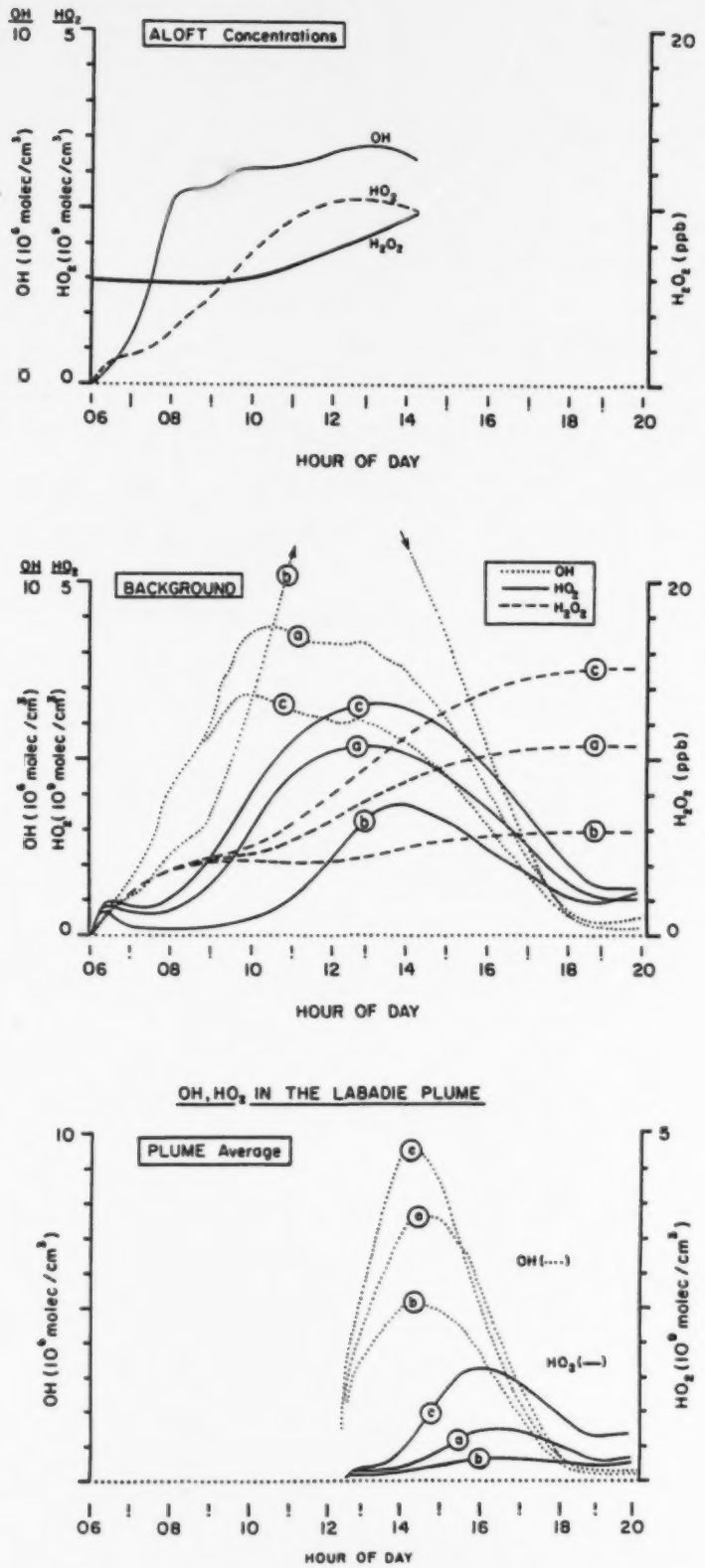

Figure 13. Dynamics of OH, HO_2, and H_2O_2 in the ambient aloft and mixing layer air, and of plume-average OH and HO_2 in the Labadie plume, corresponding to the three cases of regional emissions of NO_x and NMHC.

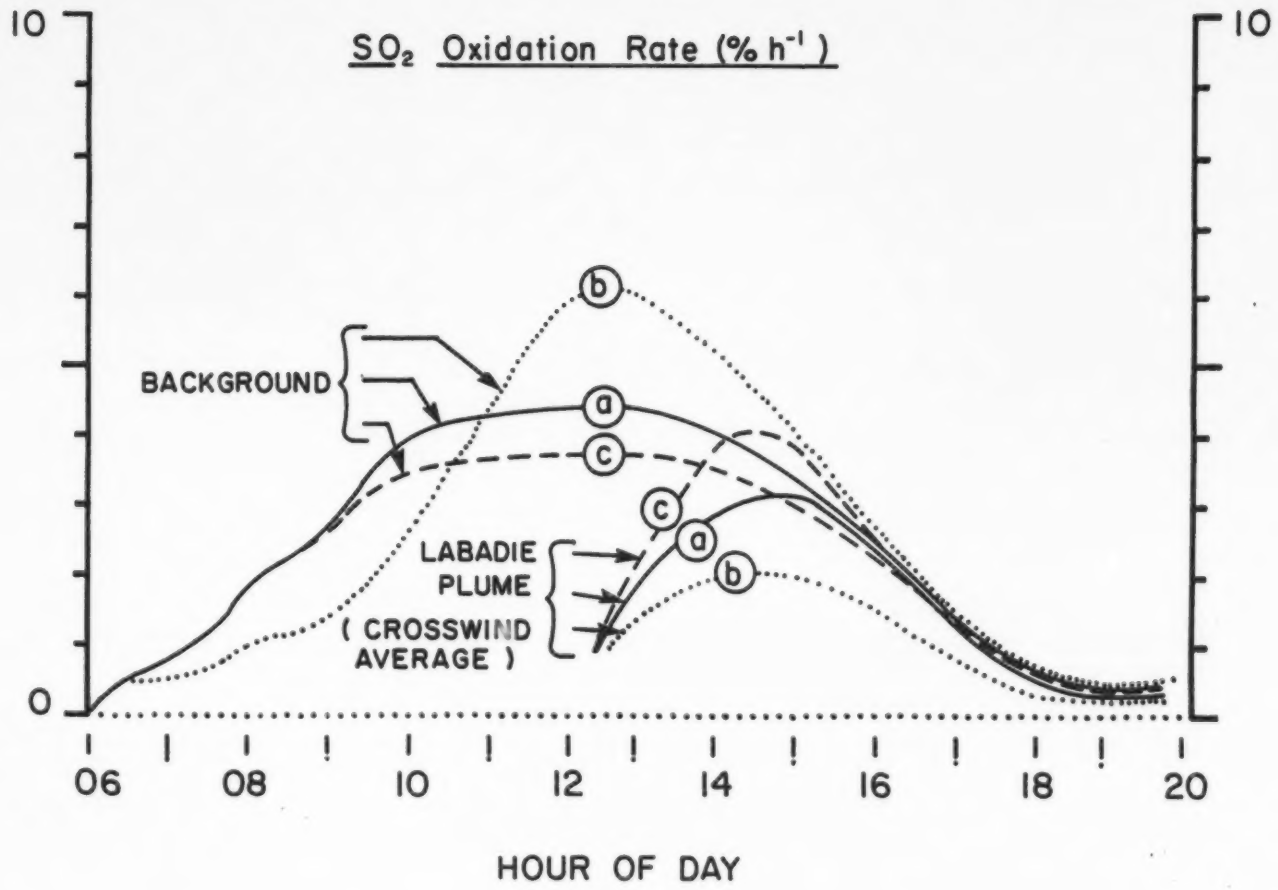

Figure 14. Rate of SO_2 oxidation in the ambient mixing layer (background) and in the Labadie plume, corresponding to the three cases of regional emissions of NO_x and NMHC.

6.5 Model Application to the Metropolitan Plume

In the model application, the full metro plume was discretized into 26 pillars. The 10 leftmost pillars represented the Labadie plume portion. Sioux power plant emissions initially (1530) dominated the contents of the next 6 pillars, and the contents of the rightmost 10 pillars initially were dominated by the remainder of the urban emissions. Figure 15 shows two cases (1c and 2c) of the initial (1530) crosswind profiles of NOx, NO_T (= NOx + HNO_3 + PAN), and NMHC, as used in two metro model simulations. The oxides of nitrogen profiles show three plumes. To the left is the Labadie plume, in the middle is principally the Sioux power plant plume, and to the right is the remaining urban plume. The initial concentration profiles include the primary emissions superimposed on the background. The three traces are identified by different symbols. The left- and right-most locations of the symbols mark the edges of the metro plume, and the data values at these points represent the background values. The other symbols, proceeding from left to right, locate the mid points of successive plume pillars. The Labadie and Sioux plume crosswind discretization was based on equal mass distribution of NOx emission of each source into the corresponding plume pillars. Thus, the width of each pillar is inversely related to the NOx concentration in the pillar, and increases outward from each plume core. The 10 urban pillars are chosen to be of equal width, and hence contain different precursor masses initially.

The initial profiles for case 1c (Figure 15 upper) are based on realistic estimates of the primary anthropogenic metropolitan emissions of NOx and NMHC superposed on the background characterized by case (c) regional emissions (determined in the previous section as most appropriate with respect to observed ozone generation in the background as well as in the Labadie plume). Case 2c (Figure 15 lower) represents another scenario of initial conditions, in which a different distribution of primary emissions are superimposed on the case (c) background. Table 2 summarizes the two primary emissions scenarios on average plume-by-plume basis.

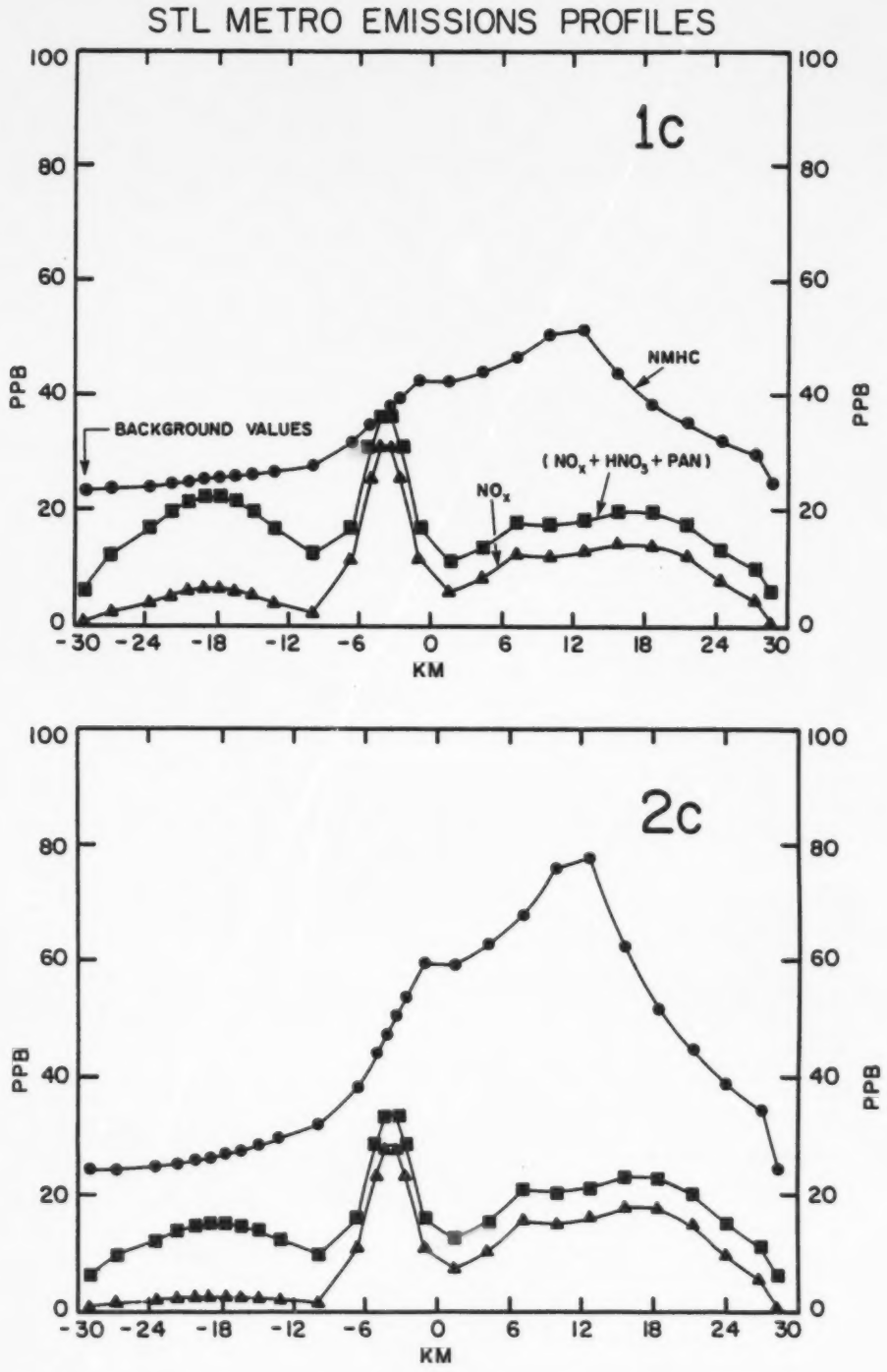

Figure 15. Initial concentration profiles (at 1530 on 9 July 1976) of the precursors for two metro St. Louis model runs. Scenario 1c corresponds to the case of realistic precursor emissions into the background characterized by the regional emissions of case c (NMHC/NOx regional flux = 8). Scenario 2c corresponds to different primary emissions into the same background. Labadie plume (at left) primary NO_x/SO_2 = 0.3 (by volume) in 1c, and 0.2 in 2c. For the urban plume (right) NMHC emissions in 2c are twice as much as in 1c. Locations of symbols coincide with pillar centers.

The NOx and NO_T profiles of the Labadie pillars in Figure 15-1c are taken as the 1530 condition of the previously described simulation of the Labadie release of 1200. The NOx profile for the remainder of the metro plume and the NMHC profile for the entire metro plume are based on the arrival at 1530 at section MM, by Monte Carlo transport, of all prior releases from each cell of the RAPS emissions inventory grid. Half-hourly releases of mass-weighted Monte Carlo dots were "followed" from 1130 onwards and past 1530. A tally was kept of dots arriving within a prescribed space surrounding section MM during a prescribed time interval around 1530. Care was taken that no Monte Carlo dot was counted more than once in the tally. The NMHC profile thus obtained was scaled up to give an integrated metropolitan mass flow rate of 9.5 kg/s (34.2 metric tons/h), which is consistent with the value used by White et al (1976) and Isaksen et al (1978). Only a small fraction of this NMHC emission is within the Labadie plume section. The urban NMHC mixing into the Sioux plume, however, is substantial. The bulk of the metropolitan NMHC emission is concentrated within the urban plume proper (the rightmost 10 pillars). The peak of its profile is downwind of the Wood River refinery complex, and the corresponding initial ratio of primary (i.e. excess over background) NMHC/NOx is about 2.2 ppbv/ppbv. To the left of the NMHC peak, the value of this excess ratio ranges between 2 and 3.4, it drops below 2 in much of the plume to the right, where the NOx peak is located. The background value of the ratio, in contrast, exceeds 35 at 1530.

The scenario in Figure 15-2c is principally different in two respects. First, in the Labadie plume, the NOx/SO_2 ratio has been reduced to 0.2 ppb/ppb, compared to 0.3 in case 1c. For most large coal-fired power plants, this ratio lies between 0.2 and 0.3. Secondly, the overall metropolitan NMHC emission has been doubled in case 2c, and its composition is adapted to that of the RAPS emissions inventory. This mixture is somewhat less reactive than that of case 1c.

The initial concentrations of species other than the primary ones are determined in the Sioux pillars by the same procedure described earlier for initialization of the Labadie plume at 1230. In the 10

Table 2

SUMMARY OF PRIMARY EMISSIONS SCENARIOS FOR THE METRO PLUME

PRIMARY EMISSIONS (kg/s)

	SCENARIO 1c[1]			SCENARIO 2c		
	Labadie	Sioux	Urban	Labadie	Sioux	Urban
SO_2	13.0	7.0	9.8	11.2	11.2	9.8
NO_x	1.88[2]	1.2[3]	3.55[4]	1.1[2]	1.1[3]	4.05[4]
NMHC	–	–	9.5[5]	–	–	19.0[6]
$NMHC/NO_x$ (By mass)			2.67			4.7
(By volume)			2.33[7]			4.1[7]
NO_x/SO_2 (By volume)	0.30	0.36	0.55	0.20	0.20	0.63

(1) Believed to be realistic

(2) As 95% NO, 5% NO_2

(3) Includes urban emissions upwind of Sioux

(4) As 25% NO, 75% NO_2

(5) As 66% paraffins, 22% aromatics, 12% olefins
This is a typical urban composition.

(6) As 72% paraffins, 18% aromatics, 10% olefins
This was the composition according to RAPS emissions inventory.

(7) Assuming molecular weight of NMHC to be 48

urban pillars, it is assumed that the ozone concentration is constant and equal to the background level. The urban plume at 1530 represents a mixture of relatively fresh releases (about one half hour old) and more aged releases (perhaps as much as three hours old). In the current version of the model, urban emissions are not aggregated dynamically within a moving, and chemically active, Lagrangian slab as it passes over the urban source area. The process is rather commenced downwind with a prescribed set of initial conditions. This is viewed as the weakest aspect of the current model, and it is also the prime target of future revision. Quite probably, there is net excess ozone in the urban plume at 1530. However, for lack of means to estimate it more accurately in the current version of the model, the constant value is assumed. It is also assumed that, at 1530, 75% of the NOx is as NO_2, and the rest is NO. The remaining species concentrations are initialized in the same manner as for the power plant plumes.

The initial crosswind profile of ozone (at 1530), and the simulated crosswind profiles at 1730 and 2000, are shown in Figure 16 for the two primary emissions scenarios. In each case, the observed ozone profile at 2000 is also shown.

The effect of urban interaction on Labadie is to shift the Labadie ozone peak closer to the urban plume, without significantly changing its intensity. Presumably, this is a combined effect of the influence of the small amount of primary NMHC directly injected into the Labadie plume at 1530 and of the entrainment/diffusion interactions between Labadie and the rest of the metro plume. This shift of the ozone peak is, however, not consistent with the observed ozone behavior in the Labadie plume. The highest observed ozone concentration in the Labadie plume actually occured farthest from the urban plume. Evidently, the urban influence on Labadie has become exaggerated in the metropolitan simulation. One possible explanation is that the sudden injection of accumulated primary NMHC into a diluted Labadie plume at 1530 gave an exaggerated NMHC/NOx value, most pronounced on the side closest to the urban plume, thereby accelerating ozone production with a spatial bias. The actual primary NMHC emissions mixing with the Labadie plume occured

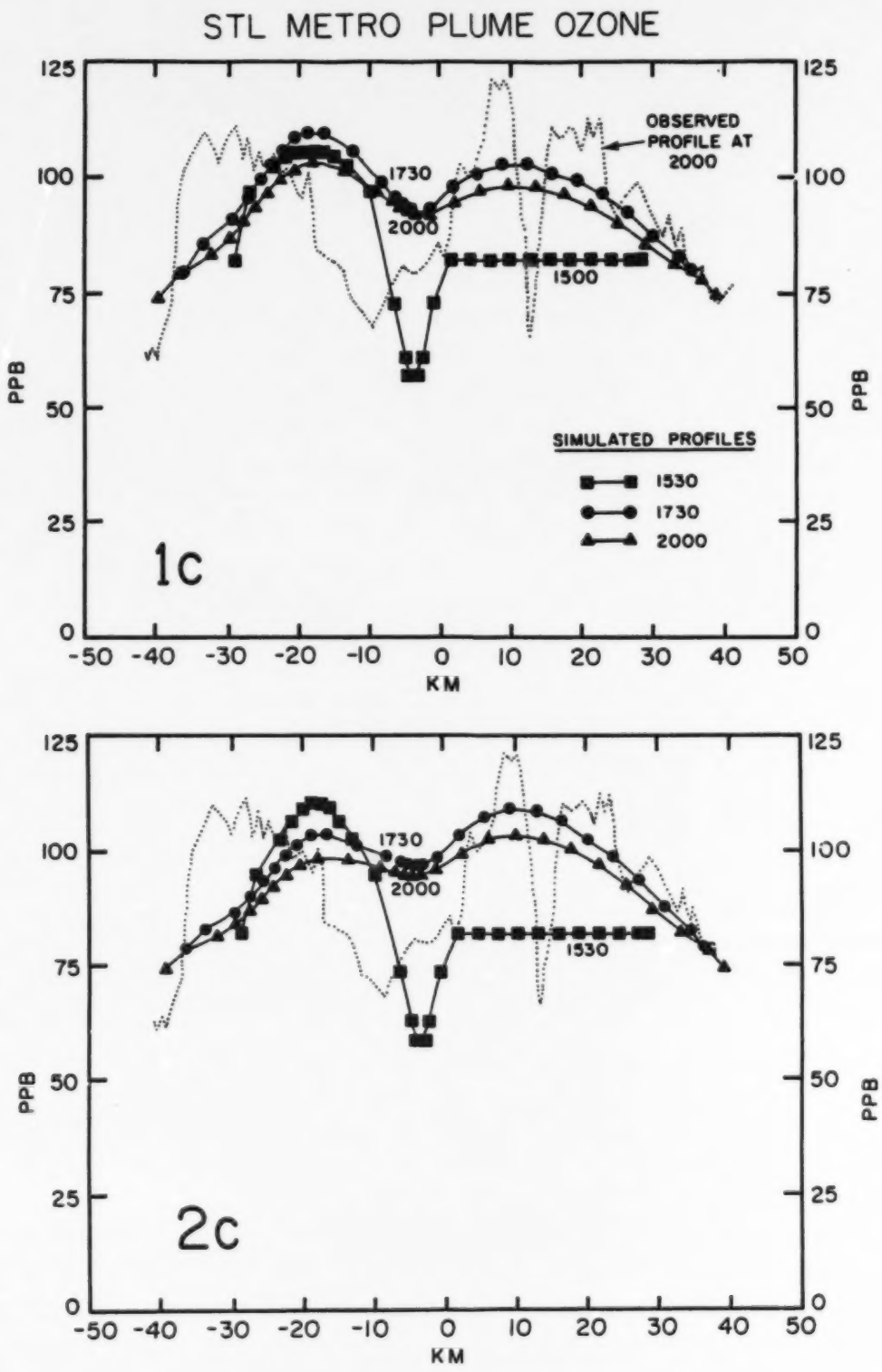

Figure 16. Evolution of simulated crosswind ozone profiles for emissions scenarios 1c and 2c of the St. Louis metro plume run for 9 July 1976. Also shown in each plot is the measured profile at about 2000.

gradually over two or more hours preceding 1530, when the Labadie plume composition was significantly different, as also was the intensity of solar radiation.

The effect of urban NMHC on the Sioux plume (the portion around the local ozone minimum between the Labadie and urban plumes) is also somewhat exaggerated in terms of faster-than-observed simulated ozone recovery in that power plant plume. This may also be partly due to the improper method of initialization. In the urban plume proper, the ozone peak is correctly located, but is somewhat smaller than the observed one. Even with the substantially boosted NMHC urban emissions in scenario 2c, the ozone peak still fell a little short of observation. The main cause of the discrepancy between observed and simulated ozone in the urban section may also be related to the initial error in the assumed constant ozone profile at 1530. The reason that the substantially increased NMHC emission of scenario 2c caused a peak boost in ozone of only about 10 ppb may be related to the fact that the plume initialization was near the end of the daytime period of photochemical activity, and that much of the extra NMHC (scenario 2c over 1c) remained unexpended at 2000 (see Figure 17, upper). In fact, the increase in scenario 1c ozone at the core of the urban plume section from about 80 ppb at 1530 to over 100 ppb within two hours near the end of the solar day reflects the responsiveness of the model.

In Figures 17 through 20, simulated details of the temporal evolution of several species in the background and at the core of the Labadie and the urban sections are presented. Figure 17 (upper) shows that at 2000, the urban plume retained substantial excess NMHC in both scenarios, partly to be used up the next day to generate more ozone within the plume (as long as adequate NOx also remains available), and partly, and more probably, to be contributed to the regional background. Figure 18 (upper) shows that in both scenarios, Labadie NOx was near background level by 2000, but that 1-2 ppb of excess NOx remained active in the urban plume for night-time chemistry and possibly also for some chemistry the next day. Such biased loading of the background by aged urban plumes must contribute significantly to typical background values of NMHC/NOx which are around 30. Aldehydes in the urban plume

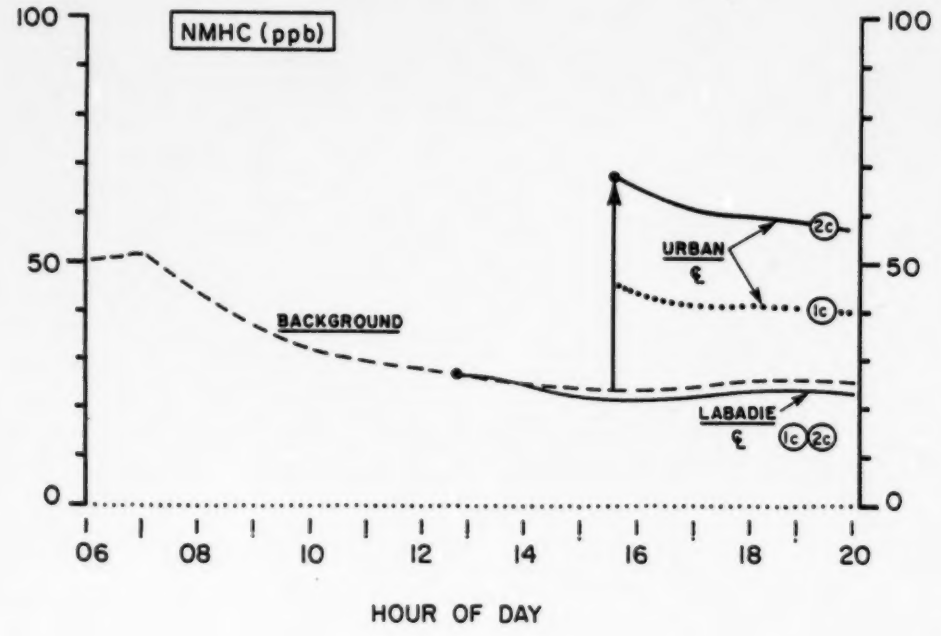

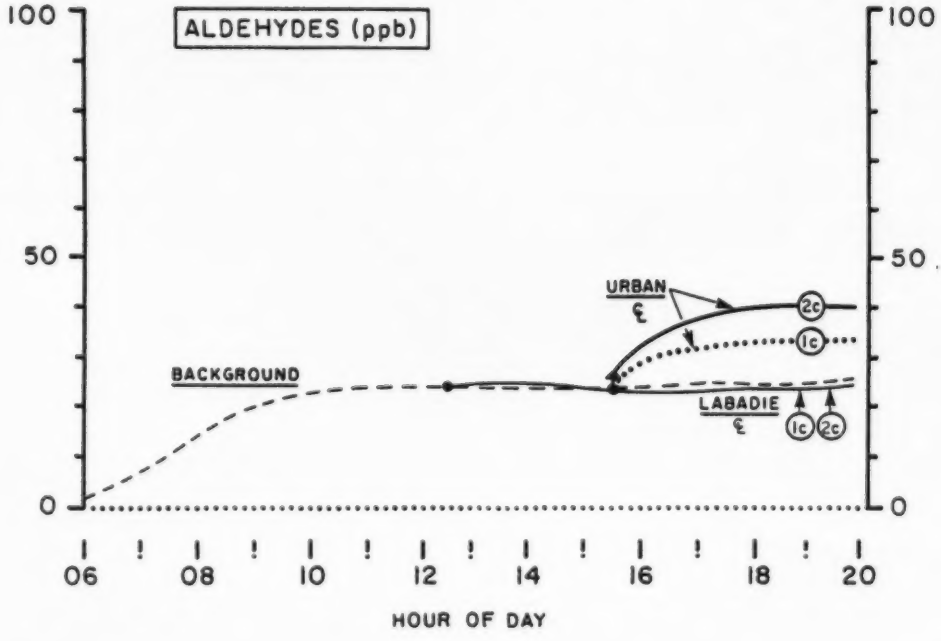

Figure 17. Dynamics of simulated concentrations of NMHC and aldehydes in the background and near the cores of the Labadie and urban plumes for the emissions scenarios 1c and 2c. Observe that much of the primary NMHC in the urban plume remains unexpended at the end of the day.

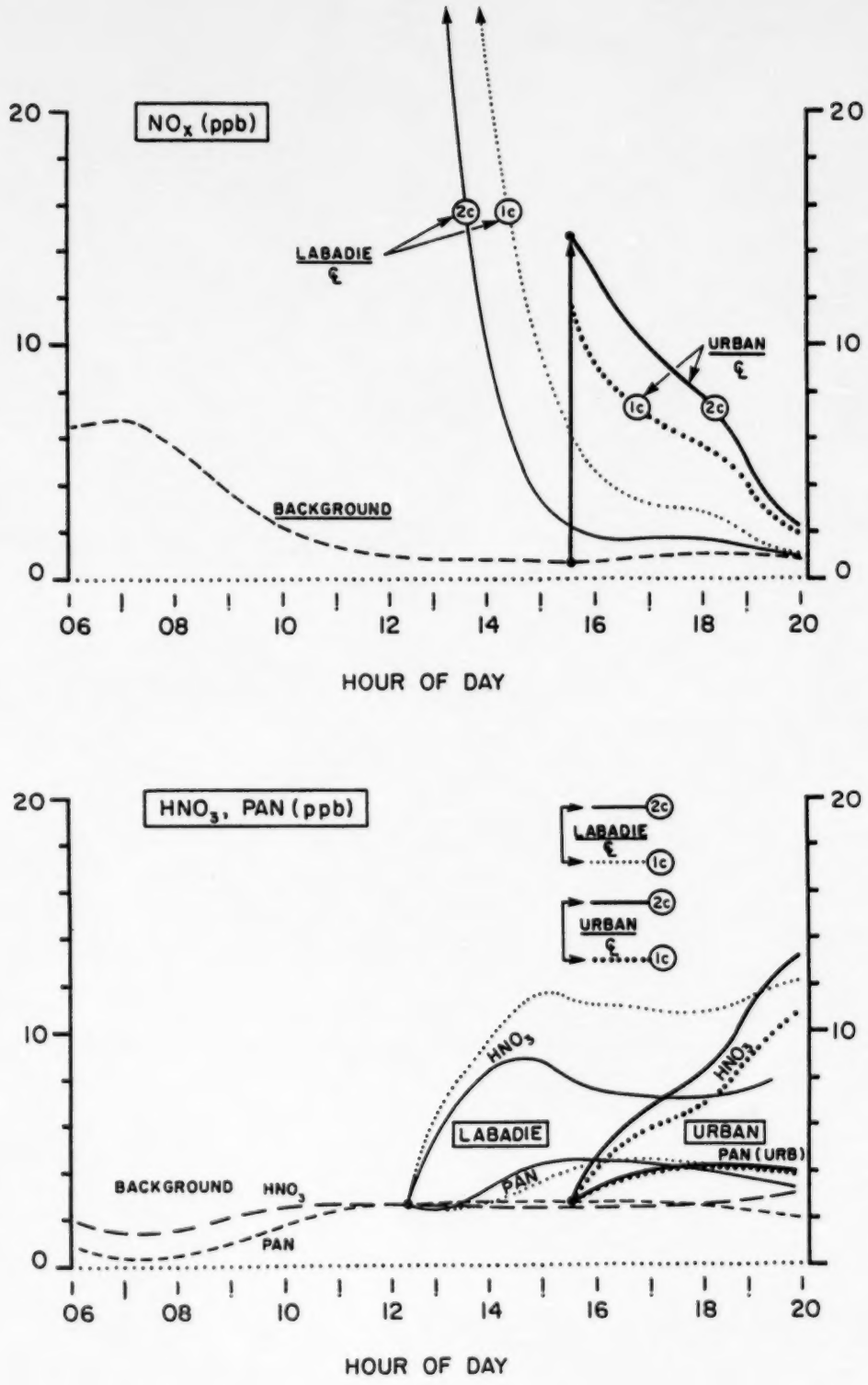

Figure 18. Dynamics of simulated concentrations of NO_x, HNO_3, and PAN in the background and near the cores of the Labadie and urban plumes for the emissions scenarios 1c and 2c.

(Figure 17 lower) show a strong dependence on initial NMHC, with substantially more being produced in scenario 2c. Figure 18 shows the temporal decrease of NOx (upper) in the two plumes, and also the formation of HNO_3 and PAN (lower). For Labadie, the HNO_3 response to initial NOx is strong, with about one-third decrease in HNO_3 (scenario 2c compared to 1c) for one-third reduction in the NOx/SO_2 ratio. Similarly, HNO_3 formation in the urban plume is also greater for the scenario with the higher initial NOx. The relatively insignificant change in urban PAN production between scenarios 1c and 2c in spite of a significant increase in the emission value of NMHC/NOx is somewhat surprising. The principal reason probably is that the urban NOx emissions are not very different in the two scenarios. Apparently, also, the increased depletion of the R_1O_2 free radicals by increased levels of NOx as well as O_3 in scenario 2c cancel out the increased production of these PAN-forming radicals from the higher level of the aldehydes, whose breakdown by OH is the principal source of R_1O_2.

The temporal behaviors of ozone and of the gas-phase oxidation rate of SO_2 in the core pillars of Labadie and of the urban plume are shown in Figure 19. For Labadie, the decreased emission of NOx in scenario 2c leads to more rapid recovery of the smaller initial ozone deficit, but in time, the ozone level drops lower than that of scenario 1c. It does not appear, however, that the amount of plume ozone depends linearly on NOx emission. The decreased NOx of scenario 2c does have a significant positive effect on the SO_2 oxidation rate in the Labadie plume, mainly because of a substantial increase in both OH and HO_2 (Figure 20). The decrease in NOx gives a corresponding increase in plume NMHC/NOx. During the early and intermediate stages of chemical development, the Labadie plume average value of the SO_2 oxidation rate is significantly greater that that at plume core, indicating more rapid SO_2 oxidation at plume edges. In the urban plume core, the relatively small increase in ozone for a much larger increase in initial NMHC/NOx in scenario 2c has been discussed before. The increased urban NMHC of scenario 2c serves to consume more OH in the last solar hours of the day, and leads to a somewhat depressed rate of SO_2 oxidation.

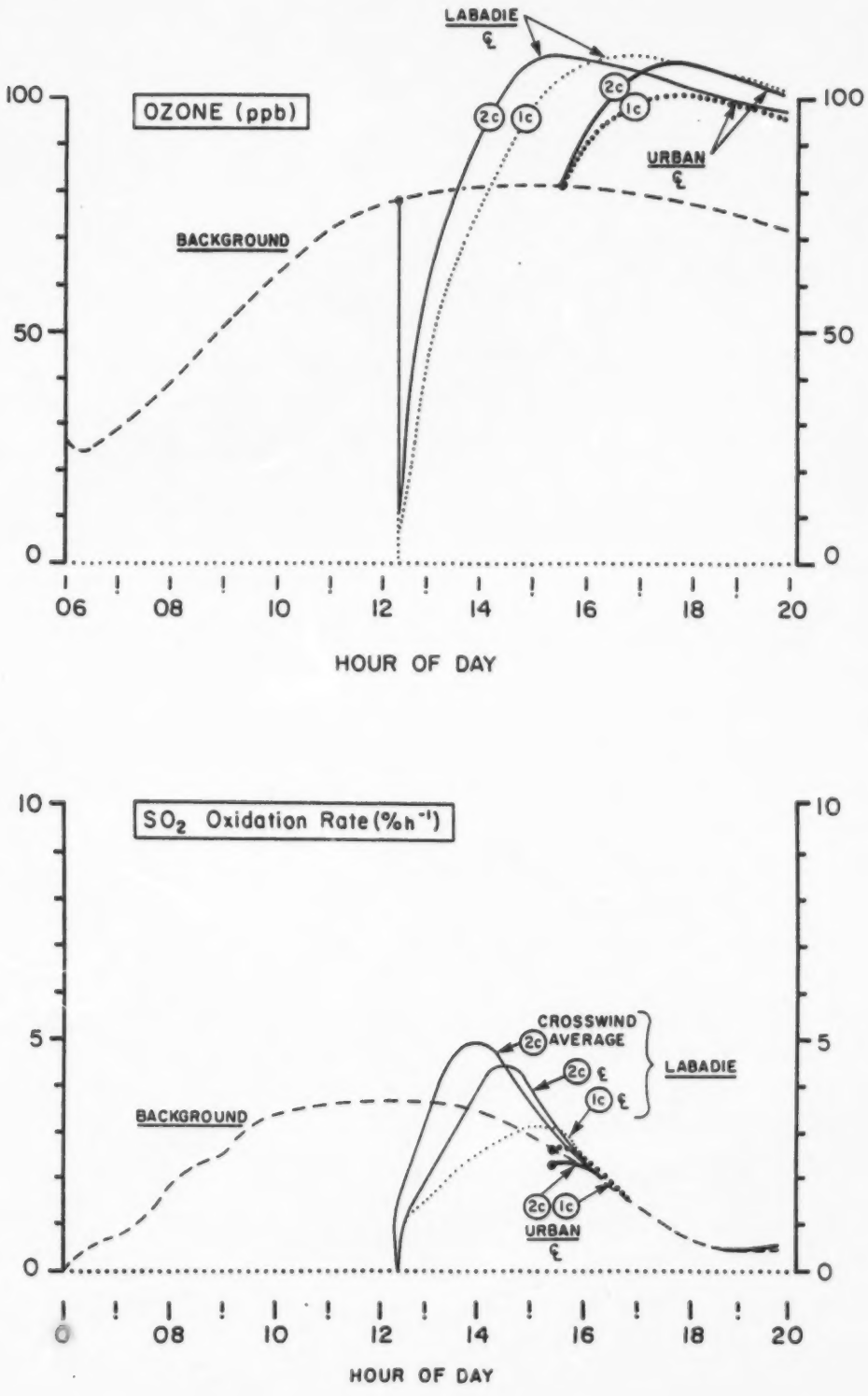

Figure 19. Dynamics of simulated concentration of O_3 and the rate of oxidation of SO_2 in the background and in the cores of the Labadie and urban plumes for the emissions scenarios 1c and 2c. Also shown is the plot of plume-average SO_2 oxidation rate in the Labadie plume.

Also shown in Figure 20 is the trend of H_2O_2 in the two plume cores for the two scenarios. In the Labadie plume, free radical depletion by NOx is less in scenario 2c because NOx is lower. The corresponding higher levels of HO_2 lead to higher levels of H_2O_2 also. In the urban plume core, on the other hand, the increased NMHC of scenario 2c towards the end of the solar day fails to generate more free radicals (in fact, presents a greater sink for them). Consequently, there is no significant increase in urban H_2O_2.

A metropolitan simulation was also run (Run 2a, results not shown) with the primary emissions of scenario 2 into the background corresponding to case (a) regional emissions. Comparison of the ozone formation in cases 2a and 2c shows a significant difference in the entire metropolitan plume (both Labadie and urban peaks remain under 100 ppb at all times in run 2a), indicating that the NMHC loading and the NMHC/NOx ratio in the background significantly influence ozone formation not only in a power plant plume, but also in an urban plume (even when the NMHC/NOx ratio in the urban plume is exaggerated as in scenario 2).

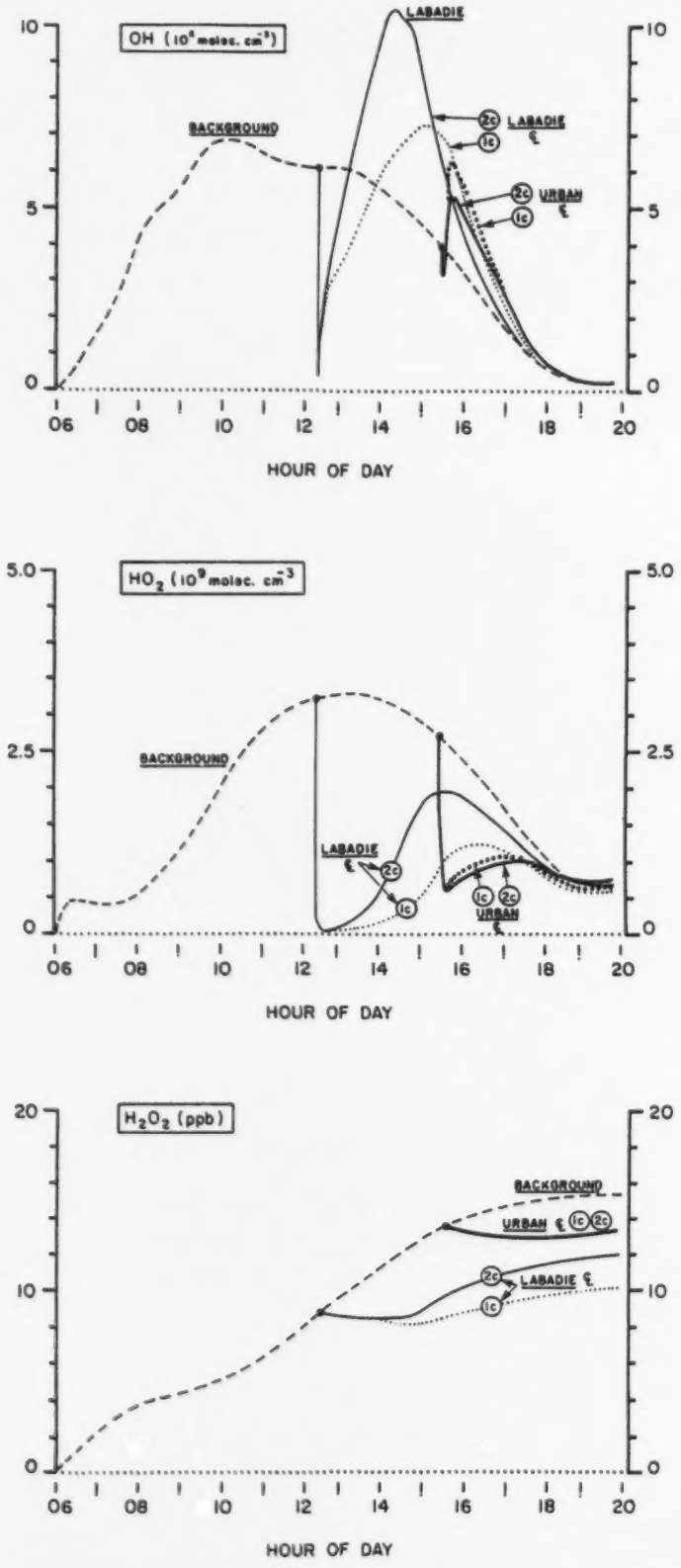

Figure 20. Dynamics of simulated concentrations of OH, HO_2 and H_2O_2 in the background and near the cores of the Labadie and urban plumes for the emissions scenarios 1c and 2c.

7. SUMMARY AND CONCLUSIONS

Documented evidence exists concerning the damaging effects of ozone on human health, forests and crops, and materials, at levels which occur frequently during summer in the ambient air in relatively polluted regions such as the eastern United States. While natural emissions of organic vapors may play a significant role in the photochemistry leading to ozone production in the atmosphere, it is evident that the predominant sources of the precursors NOx and NMHC are anthropogenic in origin. Specifically, urban-industrial complexes and power plants (many of which are located in rural areas) are the principal sources of ozone precursors. The chemistry of ozone photosynthesis in the pollutant plumes of these sources is inextricably linked also to the production of other irritants (e.g. PAN), acidic matter (e.g. H_2SO_4, HNO_3) which is responsible for acidic depositions, and fine aerosols which contribute to visibility reduction and regional haze.

The cornerstone of EPA's regulatory program for the attainment of ozone NAAQS has been the reduction of urban anthropogenic emissions of reactive organic precursors based on urban scale PAQSMs. A principal tool used in the implementation of the corresponding control strategy is the city-specific EKMA model, which attempts to relate maximum daily ozone downwind of an urban source region directly to the primary precursor emissions during the morning rush period. It has been recognized recently that the regional nature of the ozone problem must be treated within the framework of a regional PAQSM. A major current EPA effort is focused on the development of such a tool.

The impact of ozone, both local and regional, originates mostly in specific urban and rural sources. Under typical summer midday conditions in the eastern U.S., ozone photosynthesis attains a peak rather promptly and within a mesoscale range of urban sources as well as rural power plants. The regional impact follows as this peak dissapates by atmospheric dilution effects, by night-time chemistry, and by incorporation into future daytime chemistry in a multi-day regional buildup process. For a proper assessment of the problem, plume models

must quantify the phenomena of mesoscale ozone peaking and subsequent dissapation within the time scale of a day. The results of such models should be adequate for the assessment of the local problem, and must also provide the basis for sub-grid scale parameterizations to be used in regional models. Regional models can reciprocate by providing the basis for estimating the composition of the ambient environment into which the plumes are emitted.

This report is on the subject of ozone formation in pollutant plumes, both the typical urban variety and the rural power plant plumes. The investigative tools include both field observations and a new reactive plume model. The study was motivated by the need to examine and interpret available *in-situ* mesoscale data collected in metropolitan plumes in the eastern U.S. An effort was initiated to develop a plume model with spatial resolution consistent with the available field data of St. Louis RAPS and MISTT (as well as PEPE/NEROS and NEROS II), and with the capability to examine in particular the role of plume-plume and plume-background interactions. This report describes the current state of the new model and its preliminary application to a field observation scenario. The model awaits some further development which would make it fully operational and applicable to arbitrary metropolitan and rural plume emissions and their reactive transport.

7.1 Principal Features of the New Model

The principal features of the new model are outlined below:

- arbitrary crosswind resolution of the precursor emission field, as well as of the downwind concentration field;

- full dynamic interaction between typical urban plumes which are rich in NOx and NMHC, and power plant plumes which are initially devoid of NMHC, but are very rich in NOx;

- full dynamic interaction between a plume and its ambient environment;

- dynamic simulation of the ambient environment, both within the boundary layer and aloft, including the effect of regional emissions.

- the chemistry module currently uses a modified form of the Demerjian-Schere chemical scheme, and simulates the kinetics of 26 variable species in 40 reaction steps. Products include ozone, PAN, HNO_3 and H_2SO_4.

In its present state, the model is not operational in a generalized mode of application. In particular, the primary emissions module needs revision and upgrading, and the chemistry module needs to be generalized to accept any scheme. Once these revisions are implemented, an operational version of the computer code can be prepared for more general application by a wider user community.

7.2 Goals of Model Application

Model application involved the following specific goals:

- characterization of the chemical composition of the ambient environment in terms of precursors, secondary products, as well as important intermediate species (e.g. OH, HO_2, H_2O_2);

- investigation of the sensitivity of ozone photosynthesis in the background to regional emissions of the precursors;

- investigation of the sensitivity of ozone formation in a power plant plume to the composition of the ambient environment;
- simulation of the transport and chemistry of the 1200 release of the Labadie power plant plume on 9 July 1976, and comparison of the observed ozone crosswind profile 190 km downwind at 2000;

- simulation of the transport and chemistry of the metropolitan St. Louis plume, emitted over the period 1200 to 1500 on

9 July 1976, and comparison of the observed downwind ozone crosswind profile at 2000;

- simulation of the chemistry of sulfur and nitrogen oxides in the St. Louis plumes, and in the ambient environment.

7.3 Results of Model Application

The following conclusions, based on field observations and model calculations, are highlighted. They are believed to be of fairly general qualitative validity for the eastern U.S. atmosphere.

7.3.1 Ambient Environment

- The ambient environment is dynamic and chemically quite active, both in the mixing layer and aloft. It is not appropriate to assume the aloft to be quiescent during the morning period.

- The boundary layer is even more reactive, being continuously fed by regional emissions of the precursors, and by entrainment of aged air from aloft. Both effects can have strong effects in shaping boundary layer composition and chemistry.

- Afternoon values of the concentration ratio NMHC/NOx (ppbv/ppbv) of boundary layer air are around 30. In terms of ozone formation potential, such an environment is strongly NOx-limited. Regional emission flux of $2 - 3 \times 10^{11}$ molecules cm^{-2} s^{-1} of NOx appears to be appropriate for the development of about 70 ppb of ozone typically observed in the eastern U.S. summer background. This flux is consistent with the total eastern U.S. anthropogenic emissions of NOx. The depletion of NOx is quite rapid in the summer daytime atmosphere.

- The relatively high loading of NMHC in the boundary layer appears to be a result of the substantial difference in the rates of NMHC and NOx depletion in urban plumes. NOx is consumed more rapidly,

leaving behind particularly the less reactive hydrocarbons to flow and dilute into the regional background. Regional background values of NMHC in the Midwest and the Ohio River Valley region are probably around 100 ppbC (approx. 25 ppbv) on summer days.

- The formation of ozone in the background is relatively insensitive to increases in the regional emissions of NMHC. However, observed ozone formation in the Labadie plume is very sensitive to background NMHC, and requires the ratio of NMHC/NOx in the regional emission flux to be about 8 (by volume). This is considerably higher than the average eastern U.S. anthropogenic flux ratio (less than 2), but considerably less than the corresponding ambient concentration ratio on summer days (about 30). The significance of natural emissions of NMHC may be greater than previously thought.

- Production of OH, and hence the rate of SO_2 and NO_2 oxidation in the gas-phase, in the background, are strongly sensitive to ambient NOx. Gas-phase formation of acidic products in the ambient air appear to be inversely related to the concentration ratio NMHC/NOx.

7.3.2 Power Plant Plumes

- Power plant plumes are a major source of ozone in the eastern U.S. The NOx-starved and NMHC-loaded background air is very responsive to NOx loading from the power plant emissions. Following an initial depletion of ozone within the plume due to reaction with primary NO in the fresh plume, there is rapid ozone recovery and ultimately a substantial ozone bulge in the plume, as NMHC and free radical species are entrained from the background.

- The ozone-forming potential of power plant emissions is, however, strongly dependent on ambient NMHC which are not emitted by the

power plants. Presumably, while the polluted atmosphere under convective conditions is conducive to rapid ozone generation in power plant plumes, the clean atmosphere is not. An increase in ambient NOx raises ambient ozone, and reduces the potential for excess ozone formation in the plume. Ozone formation in the power plant plume is thus positively correlated with ambient NMHC/NOx.

- There is also more direct evidence of the influence of background entrainment on the evolution of plume ozone dynamics. The developing crosswind profiles clearly show that plume ozone recovery is most rapid in plume edges where the NMHC/NOx ratio is highest.

- It appears that the ozone recovery in the plume is complete approximately when the cross-sectional average value of NMHC/NOx in the plume exceeds about 1 ppbv/ppbv.

- The rates of oxidation of SO_2 and NO_2 in the plume appear to be positively correlated with ambient NMHC/NOx. This correlation for SO_2 appears to be much better than the correlation of the SO_2 oxidation rate with ambient ozone. Hence, use of ambient ozone as a surrogate for ambient NMHC/NOx in parameterizations of the SO_2 oxidation rate is not well founded. However, given the dearth of reliable ambient data of NMHC and NOx, and the approximate level of accuracy of estimates of the SO_2 oxidation rate based on field measurements, the continued temporary use of ozone may be justifiable in empirical parameterizations.

7.3.3 Metropolitan Plumes

- Urban emissions are rich in both precursors of ozone, and hence, urban plumes are less reliant on background entrainment for ozone photosynthesis than are power plant plumes.

- Metropolitan emissions are typically characterized by a diverse spatial distribution of the precursor mix, and of source configurations. There is a corresponding wide range of spatial-temporal variability of ozone distribution. There is good evidence for the "source intensification" effect where plumes intersect. Improper treatment of the primary emissions distribution does lead to distortion of the ozone distribution. Urban emisions are capable of generating substantial amounts of ozone rapidly. The production of ozone then slows down as the NOx becomes depleted long before the NMHC, thus passing on a substantial excess of NMHC to the regional background. This relative overloading of the background remains potent in terms of ozone production. This potential is realized when NOx emissions are released into the background.

7.3.4 General

- Proper chemical characterization of the primary emission field and of the ambient environment remain high priority needs for reliable prediction of ozone formation in the polluted atmosphere.

- The city-specific EKMA appears to have some serious shortcomings which need to be further investigated.

- Sub-grid scale effects are very important near precursor sources in the context of regional models. Mesoscale field observations and model applications must be directed at the study and quantification of such effects.

REFERENCES

Bazzell C.C. and L.K. Peters (1981). The transport of photochemical pollutants to the background troposphere. *Atmospheric Environment* 15, 957-968.

Clark T.L. (1980). Annual anthropogenic pollutant emissions in the United States and southern Canada east of the Rocky Mountains. *Atmospheric Environment* 14, 961-970.

Clark T.L. and J.F. Clarke (1984). A Lagrangian study of the boundary layer transport of pollutants in the northeastern United States. *Atmospheric Environment* 18, 287-298.

Demerjian K.L. and K.L. Schere (1979). Applications of a photochemical box model for ozone air quality in Houston, Texas. Proc., Specialty Conf. on Ozone/Oxidants: Interactions with the Total Environment II, Houston, Texas, 14-17 October, 1979.

Demerjian K.L., K.L. Schere and J.T. Peterson (1980). Theoretical estimates of actinic flux and photolytic rate constants of atmospheric species in the lower troposphere. Adv. Environ. Sci. Technol. 10, J. Pitts and R. Metcalf (eds), J. Wiley & Sons, Inc., 369-459.

Dimitriades B. (1978). Dependence of ambient oxidant/ozone precursor control. Paper presented at the 85th National AIChE Meeting, Philadelphia, PA, 4-8 June, 1978.

Dodge M. C. (1984). Combined effects of organic reactivity and NMHC/NO_x ratio on photochemical oxidant formation — a modeling study. *Atmospheric Environment* 18, 1657-1665.

EPA (1977a). Proc., EPA Symp. Northeast Oxidant Study. EPA-600/3-77-017.

EPA (1977b). Uses, limitations and technical basis of procedures for quantifying relationships between photochemical oxidants and precursors. EPA-450/2-77-021a.

EPA (1978). Procedures for quantifying relationships between photochemical oxidants and precursors: supporting documentation. EPA-450/2-77-021b.

EPA (1980). Guideline for use of city-specific EKMA in preparing ozone SIPs. EPA-450/4-80-027.

Farrow L.A. and D. Edelson (1974). The steady-state approximation: fact or fiction? *Int. J. Chem. Kin.* VI, 787-800.

Fishman J. and P.J. Crutzen (1978). The origin of ozone in the troposphere. *Nature* 274, 855-858.

Fishman J., F.M. Vukovich and E.V. Browell (1985). The photochemistry of synoptic-scale ozone sythesis: implications for the global tropospheric ozone budget. To be published in *J. Atmospheric Chemistry*.

Gear C.W. (1971). The automatic integration of ordinary differential equations. *Comm. A.C.M.* 14, 176-179.

Gillani N.V. (1978). Project MISTT: mesoscale plume modeling of the dispersion, transformation, and ground removal of SO_2. *Atmospheric Environment* 12, 569-588.

Gillani N.V., R.B. Husar, J.D. Husar and D.E. Patterson (1978). Project MISTT: kinetics of particulate sulfur formation in a power plant plume out to 300 km. *Atmospheric Environment* 12, 589-598.

Gillani N.V. and W.E. Wilson (1980). Formation and transport of ozone and aerosols in power plant plumes. Annals N.Y. Acad. Sci. 338, 276-296.

Gillani N.V., S. Kohli and W.E. Wilson (1981). Gas-to-particle conversion of sulfur in power plant plumes: I. Parameterization of the conversion rate for dry, moderately-polluted ambient conditions. *Atmospheric Environment* 15, 2293-2314.

Gillani N.V. and W.E. Wilson (1985). Project MISTT: measurements and data base. To be published as EPA technical report.

Gipson G.L. (1984). Application and comparison of three photochemical models: urban airshed, EKMA/Dodge, EKMA/CB-3. Paper No. 84-47.8, 77th Annual Meeting, APCA, San Francisco, CA, 24-29 June, 1984.

Hesstvedt E., O. Hov and I.S.A. Isaksen (1978). Quasi-steady-state approximations in air pollution modeling: comparison of two numerical schemes for oxidant prediction. *Int. J. Chem. Kin.* X, 971-994.

Hov O. and I.S.A. Isaksen (1981). Generation of secondary pollutants in a power plant plume: a model study. *Atmospheric Environment* 15, 2367-2376.

Hov O. (1983). Numerical solution of a simplified form of the diffusion equation for chemically reactive atmospheric species. *Atmospheric Environment* 17, 551-562.

Killus J.P. and G.Z. Whitten (1982). A new carbon-bond mechanism for air quality simulation modeling. EPA-600/3-82-041.

Killus J.P. and G.Z. Whitten (1984). Effects of photochemical kinetic mechanisms on oxidant model predictions. Paper No. 84-114 P.2, 77th Annual Meeting, APCA, San Francisco, CA, 24-29 June, 1984.

Levine S.Z. and S.E. Schwartz (1983). Construction and testing of a Surrogate CHEmical MEchanism (SCHEME) for tropospheric photochemical reactions. In Trace Atmospheric Constituents, S.E. Schwartz (ed.), Wiley-Interscience, 455-492.

Lurman F., D. Godden, C. Lloyd and R.A. Nordsieck (1979). A Lagrangian photochemical air quality simulation model: adaptation to the St. Louis RAPS data base. Vol. I. Model formulation. ERT, Westlake, CA.

Miller D.F., A.J. Alkezweeny, J.M. Hales and R.N. Lee (1978). Ozone formation related to power plant emissions. *Science* 202, 1186-1188.

Miller D.F. and A.J. Alkezweeny (1980). Aerosol formation in urban plumes over Lake Michigan. Annals of N.Y. Acad. Sci. 338, 219-232.

Reynolds S.D. and L.E. Reid (1978). An introduction to the SAI Airshed Model and its usage. SAI Ef 78-53R, Systems Applications, Inc., San Rafael, CA.

Reynolds S.D., L. Reid, M. Hillyer, J.P. Killus, T.W. Tesche, R.I. Pollack, G.E. Anderson and J. Ames (1979). Photochemical modeling of transportation control strategies: Vol. I. Model development, performance evaluation, and strategy assessment. Systems Applications Inc., San Rafael, CA.

Schere K.L. and N.C. Possiel (1984). U.S. EPA Regional Oxidant Model — background and overview. Paper No. 84-47.2, 77th Annual Meeting, APCA, San Francisco, CA, 24-29 June, 1984.

Schere K.L. and J.H. Schreffler (1982a). Evaluation of four urban-scale photochemical air quality simulation models. EPA-600/3-82-043.

Schere K.L. and J.H. Schreffler (1982b). Final evaluation of four urban-scale photochemical air quality simulation models. EPA-600/3-82-094.

Schuck E.A., A.P. Altshuller, D.S. Barth and G.B. Morgan (1970). Relationship of hydrocarbons to oxidants in ambient atmospheres. *J. APCA* 20, 297-302.

Sexton K. and H. Westberg (1983). Photochemical ozone formation in urban and point-source plumes. *Environ. Sci. Technol.* 17, 224-227.

Spicer C.W., D.W. Joseph, P.R. Sticksel and G.F. Ward (1979). Ozone sources and transport in the northeastern United States. *Environ. Sci. Technol.* 13, 975-985.

Spicer C.W. (1981). Nitrogen oxide reactions in the urban plume of Boston. *Science* 215, 1095-1097.

Spicer C.W., D.W. Joseph and P.R. Sticksel (1982). An investigation of the ozone plume from a small city. *J. APCA* 32, 278-281.

Stewart D.A. and M.K. Liu (1981). Development and application of a reactive plume model. *Atmospheric Environment* 15, 2377-2393.

Stockwell W.R. and J.G. Calvert (1983). The mechanism of the HO-SO_2 reaction. *Atmospheric Environment* 17, 2231-2236.

Strothman J.A. and F.A. Schiermeier (1979). Documentation of the RAPS and related investigations in the St. Louis Air Quality Control Region. EPA-600/4-79-076.

Vukovich F.M., J. Fishman and E.V. Browell (1985). The reservoir of ozone in the boundary layer of the eastern United States and its potential impact on the global tropospheric ozone budget. *J. Geophys. Res.* 90 (D3), 5687-5698.

White W.H., J.A. Anderson, D.L. Blumenthal, R.B. Husar, N.V. Gillani, J.D. Husar and W.E. Wilson, Jr. (1976). Formation and transport of secondary air pollutants: ozone and aerosols in the St. Louis urban plume. *Science* 194, 187-189.

White W.H. (1977). NO_x-O_3 photochemistry in power plant plumes: comparison of theory with observation. *Environ. Sci. Technol.* 11, 995-1000.

White W.H. and D.E. Patterson (1983). Dispersion, mixing, and chemical reaction in a heterogeneous urban-industrial plume. Paper No. 83-31.5, 76th Annual Meeting, APCA, Atlanta, GA.

White W.H., D.E. Patterson and W.E. Wilson (1983). Urban exports to the non-urban troposphere: results from Project MISTT. *J. Geophys. Res.* 88 (C15), 10745-10752.

Whitten G.Z. and H. Hogo (1978). Users manual for kinetics model and ozone isopleth plotting package. EPA-600/8-78-014a.

Wolff G.T., P.J. Lioy, R.E. Meyers and R.T. Cederwall (1977). Anatomy of two ozone transport episodes in the Washington, DC to Boston, MA Corridor. *Environ. Sci. Technol.* 11, 506-510.